WADD TECHNICAL REPORT 60-906

Research on the Distribution of Tension in Notched Construction Parts

Professor Dr. -Ing. H. Neuber

Technische Hochschule
Munchen, Germany

January 1961

Materials Central
Contract No. AF 61(514)-1111
Project No. 7360

Wright Air Development Division
Air Research and Development Command
United States Air Force
Wright-Patterson Air Force Base, Ohio

AF-EGLIN AFB, FLA

FOREWORD

This report was prepared in the Technische Hochschule Munchen, Germany, Institut für Technische Mechanik under USAF Contract No. AF 61(514)-1111. The contract was initiated under Project No. 7360, "Materials Analysis and Evaluation Techniques", Task No. 73605, "Design Data for Metals." The research was administered under the direction of the Materials Central, Directorate of Advanced Systems Technology, Wright Air Development Division, with Dr. A. J. Herzog acting as project engineer.

This report covers work during the period from December 1956 through January 1959.

The author and his coworkers wish to express appreciation to Capt. W. R. Yost and Capt. C. C. La Plante of the European Office in Brussels, Belgium for their support and cooperation.

My coworkers, Dr. -Ing. H. Bufler and Dipl. Phys. H. G. Hahn, contributed to the theoretical work and also prepared the manuscript of this report. The experimental investigations were carried out by Dipl. Ing. E. Krempl and others.

ABSTRACT

The influence of various factors (notch-radius, depth of notch, notch-angle, material) on the stress concentration of notched flat bars was investigated theoretically and experimentally. The aim of the research work was the extension and completion of the methods available for the calculation of stresses in notched structural elements.

For the experimental determination of the strains and stresses mainly electrical strain gages were used; in addition to that measurements were made by means of the photoelastic stress-coat method.

In the considered cases the elastic stress-concentration factors, and the stress distribution over the minimum cross section were evaluated theoretically and experimentally for the elastic range. For the plastic range a method was developed taking into consideration the real stress-strain curve of the material. This method allows the calculation of the stress concentration factor (which is known to decrease with increasing load) in dependence of the nominal stress in tension and bending. We have evaluated in this way diagrams for four different materials (steel St. 00.12, St. 00.21, pure Aluminum, and Aluminum alloy "Velodur"), which show the SCF vs. the nominal stress. Numerous tests with notched specimens of the above mentioned materials confirm the theory. In these tests in the plastic range the strain distribution over the minimum cross section also was determined. Further theoretical investigations concern the treatment of V-shaped notches and the influence of the notch-angle in pure shear.

PUBLICATION REVIEW

This report has been reviewed and is approved.

FOR THE COMMANDER:

JOSEPH M. PAGANO, MAJOR USAF
Acting Chief, Advanced Metallurgical Studies Branch
Metals & Ceramics Laboratory
Materials Central

TABLE OF CONTENTS

GLOSSARY OF SYMBOLS

α	stress concentration factor in the elastic range (ESCF)
ρ	radius of curvature of the notch
a, t	dimensions of the notch (cf. Fig. 23)
d	thickness of the specimen
F	area of the minimum cross section
ω	notch-angle
E	Young's modulus
$1/\nu$	Poisson's ratio
η	material constant with the dimension of a length which appears in the theory of V-shaped notches
P	tensile force
M	bending moment
x, y	rectangular Cartesian coordinates
σ	normal stress
σ_{MAX}	real stress in the notch
σ_N	nominal stress in the linear theory (corresponding to the minimum cross section)
σ_N^*	non-linear nominal stress
σ_i	maximum stress in the linear theory
σ_W	real s tress (corresponding to stress-strain curve)
σ_E	substitute stress (according the non-linear deformation law)
σ^*	parameter with the dimension of a stress
τ_H	principal shear stress
ε	strain
δ	order of isochromatics
S	photoelastic constant
R	electrical resistance

(All other symbols are explained in the text)

LIST OF TABLES

LIST OF ILLUSTRATIONS

LIST OF ILLUSTRATIONS (continued)

LIST OF ILLUSTRATIONS (continued)

LIST OF ILLUSTRATIONS (continued)

LIST OF ILLUSTRATIONS (continued)

I. INTRODUCTION*

It is well known that the loading of notched parts produces stress concentrations around the notches. The solution of these problems is very important for the proper design of structural elements. This is especially important in the case of lightmetal engineering where the constituent parts are used to its full strength in order to save weight. Therefore the knowledge of stress and strain in the plastic range too is indispensable.

Therefore a few of the basic problems connected with simple plane notches had been investigated experimentally and theoretically. The experimental work consists mainly of strain measurements carried out with electrical strain gages and additional photoelastic measurements by means of the so-called stress-coat method.
The theoretical investigations deal essentially with the determination of stress concentration in the elastic and plastic range. For the plastic range, a new method had to be developed. Besides there were made theoretical investigations of V-shaped notches.

---

* Manuscript released by the author on 25 February 1959 for Publication as a WADD Technical Report

II. THEORETICAL PART

The theoretical work is divided into two sections concerning the elastic and the plastic range. In the elastic range the stress concentration essentially depends upon the shape of the notch, while in the plastic range the stress-strain curve of the material must be taken into consideration.

1. Elastic Range

1.1. Elastic Stress Concentration Factors

The stress concentration factor in the elastic range (ESCF) for arbitrarily deep notches can be calculated by the interpolation of the ESCF of the deep hyperbolic notch (α_t) and the flat elliptic notch (α_f) as given by H. Neuber [1] *)

$$\alpha = 1 + \frac{(\alpha_f - 1)(\alpha_t - 1)}{\sqrt{(\alpha_f - 1)^2 + (\alpha_t - 1)^2}} \tag{1}$$

The dependence of the ESCF on a/ρ had been calculated for the experimentally investigated strips by eq.(1). It follows from the theory that for the double-sided deep hyperbolic notch in tension

$$\alpha_t = \frac{2\left(\frac{a}{\rho}+1\right)\sqrt{\frac{a}{\rho}}}{\left(\frac{a}{\rho}+1\right)\arctan\sqrt{\frac{a}{\rho}} + \sqrt{\frac{a}{\rho}}} \tag{2}$$

and for the single or double-sided flat elliptic external notch in tension and bending

$$\alpha_f = 1 + 2\sqrt{\frac{t}{\rho}} \tag{3}$$

*) Numbers in parentheses refer to references in the Bibliography

The ESCF which is calculated in this way for a tension strip with a pair of semicircular notches is shown vs. ρ/a in Fig.26. Further in this figure are plotted the theoretical values as calculated from the equations of Ling [2] and Isida [3].

For the <u>one-sided deep hyperbolic notch in bending</u>

$$\alpha_t = \frac{2\left(\frac{a}{\rho}+1\right) - \alpha_1\sqrt{\frac{a}{\rho}+1}}{\frac{4}{\alpha_2}\left(\frac{a}{\rho}+1\right) - 3\alpha_1} \qquad (4)$$

with $\alpha_1 = \dfrac{2\left(\frac{a}{\rho}+1\right)\sqrt{\frac{a}{\rho}}}{\left(\frac{a}{\rho}+1\right)\arctan\sqrt{\frac{a}{\rho}} + \sqrt{\frac{a}{\rho}}}$ and $\alpha_2 = \dfrac{4\,\frac{a}{\rho}\sqrt{\frac{a}{\rho}}}{3\left[\left(\frac{a}{\rho}-1\right)\arctan\sqrt{\frac{a}{\rho}} + \sqrt{\frac{a}{\rho}}\right]}$

Again eq.(3) is also valid for the <u>flat external notch</u>.

In the same way one can also calculate for a <u>deep internal notch in tension</u>

$$\alpha_t = \frac{\alpha_1 - 2C}{1 - \frac{C}{\sqrt{\frac{a}{\rho}+1}}} + \frac{2\left(\frac{a}{\rho}+1\right) - \alpha_1\sqrt{\frac{a}{\rho}+1}}{\frac{4}{\alpha_2}\left(\frac{a}{\rho}+1\right) - 3\alpha_1} \qquad (5)$$

with

$$C = \frac{\alpha_1 - \sqrt{\frac{a}{\rho}+1}}{\frac{4}{3\alpha_2}\sqrt{\frac{a}{\rho}+1} - 1}$$

$$\alpha_1 = \frac{2\left(\frac{a}{\rho}+1\right)\sqrt{\frac{a}{\rho}}}{\left(\frac{a}{\rho}+1\right)\arctan\sqrt{\frac{a}{\rho}} + \sqrt{\frac{a}{\rho}}} \qquad \alpha_2 = \frac{4\,\frac{a}{\rho}\sqrt{\frac{a}{\rho}}}{3\left[\left(\frac{a}{\rho}-1\right)\arctan\sqrt{\frac{a}{\rho}} + \sqrt{\frac{a}{\rho}}\right]}$$

For the flat internal notch again eq.(3) is valid. In the case of doubly connected regions, the value of

$$\alpha' = e^{0,35\, a/t} \qquad (6)$$

must be added to the ESCF α which is calculated from eq.(1). In this manner the ESCF was calculated for tension strips with a central hole and the curve ESCF vs. a/ρ is shown in Fig.27. The experimental results confirm the validity of this theory and also the rigorous solution by Howland [4]. The curve as calculated from the equations of Howland is also shown in Fig.27 for comparison.

1.2. Notch-angle Theory for Shear

In a refined consideration the ESCF is dependent not only on the "notch-curvature" a/ρ but also on the notch-angle ω which comes in as a new parameter. The notch-angle theory had been at present established for the extreme cases of flat and deep notches under pure shear assumptions. The result of these rather extensive calculations is shown in Fig.1.

With Fig.1 and eq.(1) the ESCF can be evaluated for a strip with a notch of arbitrary depth and arbitrary notch-angle in shearing. The result for the size of the bending bar according Fig. 23C ($a/\rho = 5$, $t/\rho = 1$) is shown in Fig.28 together with the measurement values of our bending tests.

1.3. Stress Distribution over the Minimum Section

Since the stress gradient near the notch exerts considerable influence on the fatigue strength of the material, the knowledge of the stress distribution over the minimum section attains more importance. The theory yields the exact stress

distribution for the double-sided deep hyperbolic notch. All these formulas can be naturally used as the first approximation for the practical notches. But one can also attain a better approximation in the following way. For a particular practical notch, for instance a tension strip with a pair of symmetrical semicircular notches (see Fig. 23A), one uses either the theoretical or experimental ESCF α . Now this is compared with a hyperbolic notch with notch radius ρ^* and ESCF α^* . Using the condition that $\alpha = \alpha^*$ it can be calculated the value of the "modified notch-radius" ρ^* using eq.(2).

Now for the practical notches the formula of the stress-distribution over the minimum section for the deep hyperbolic notches in tension can be applied

$$\frac{\sigma_y}{\sigma_N} = \frac{\left(\frac{a}{\rho^*}+1\right)\sqrt{\frac{a}{\rho^*}}}{\left(\frac{a}{\rho^*}+1\right)\arctan\sqrt{\frac{a}{\rho^*}}+\sqrt{\frac{a}{\rho^*}}} \cdot \frac{2+\frac{a}{\rho^*}\left[1-\left(\frac{x}{a}\right)^2\right]}{\left\{1+\frac{a}{\rho^*}\left[1-\left(\frac{x}{a}\right)^2\right]\right\}^{3/2}} \qquad (7)$$

In this way there follows for instance for a tension strip with a pair of symmetrical semicircular notches ($a/\rho = 2$) from the experimentally determined ESCF $\alpha = 2{,}06$ the value $a/\rho^* = 2{,}19$ and by means of eq.(7) the stress distribution shown in Fig. 34 A, which is in good agreement with the experimental results.

For the stress distribution over the minimum section of an one-sided hyperbolic notched bar subjected to a bending moment, we find

$$\frac{\sigma_y}{A} = \left[\sqrt{\frac{a}{\rho^*}+1} - \left(1+\frac{\frac{a}{\rho^*}+1}{\sqrt{\frac{a}{\rho^*}}}\arctan\sqrt{\frac{a}{\rho^*}}\right)\cdot\frac{x}{a}\right] \cdot \frac{2+\frac{a}{\rho^*}\left[1-\left(\frac{x}{a}\right)^2\right]}{\left\{1+\frac{a}{\rho^*}\left[1-\left(\frac{x}{a}\right)^2\right]\right\}^{3/2}} \qquad (8)$$

with

$$A = \frac{\sigma_N}{\sigma} \frac{1}{1 - \frac{1}{2\frac{a}{\rho^*}}\left(1 + \frac{\frac{a}{\rho^*}+1}{\sqrt{\frac{a}{\rho^*}}} \arctan\sqrt{\frac{a}{\rho^*}}\right)\left(1 + \frac{\frac{a}{\rho^*}-1}{\sqrt{\frac{a}{\rho^*}}} \arctan\sqrt{\frac{a}{\rho^*}}\right)}$$

For example, it can be shown that for a notch with $a/\rho = 5$ and the experimentally determined ESCF $\alpha = 2{,}01$ there follows from eq.(4) the value $a/\rho^* = 4{,}0$. The stress distribution according to eq.(8) is shown in Fig. 37A, which shows remarkable agreement with the experimental results.

1.4. Theory of V-shaped Notches

In the case of notches with very small radius ρ and especially with V-shaped notches ($\rho = 0$), the classical theory of elasticity gives too great values of the ESCF. Therefore it is necessary to introduce a new material constant η , which represents the dimension of a small material-particle, for example a small crystal grain (see Fig.2). The theory shows that there exists a relation between the real notch radius ρ and the fictitious radius ρ_1 with the notch angle ω as a parameter. The radius ρ has to be replaced by ρ_1 in the case of very small notches.

For <u>pure shear</u> there is valid

$$\left[\left(1-\frac{1}{q}\right)\rho_1\right]^{\frac{1}{q}-1} = \frac{q}{\eta}\left\{\left[\left(1-\frac{1}{q}\right)\rho+\eta\right]^{\frac{1}{q}} - \left[\left(1-\frac{1}{q}\right)\rho\right]^{\frac{1}{q}}\right\} \qquad (9)$$

with $$q = 2 - \frac{\omega}{\pi}$$

and for pure tension

$$\rho_1^{\frac{r-q}{q}} = \frac{q-1}{(q+r-1)\eta}\left[\left(\rho+\frac{q}{q-1}\eta\right)^{\frac{r}{q}}-\left(\rho+\frac{q}{q-1}\eta\right)^{\frac{1-q}{q}}\cdot\rho^{\frac{r+q-1}{q}}\right] \quad (10)$$

and the relation between r and q is given by

$$r = 1+\frac{q}{2}-\sqrt{2q-\frac{7}{4}} \quad (11)$$

The relations (9) and (10) are shown in Figs.3 and 4.

For the special case $\omega = 0$, the relations between ρ and ρ_1 reduce to a simpler form.

For pure shear there follows

$$\rho_1 = \frac{1}{4}\left(\sqrt{\rho+2\eta}+\sqrt{\rho}\right)^2 \quad (12)$$

and for pure tension

$$\rho_1 = \rho+2\eta \quad (13)$$

In the case of V-shaped notches ($\rho = 0$), the dependence of ρ_1/η on the notch-angle ω for pure shear and tension as evaluated from eqs.(9) and (10) is shown in Figs. 5 and 6. In the theoretical treatment of V-shaped notches, the value of ρ_1 instead of ρ has to be inserted in the formulas for the ESCF. The constant η is dependent on the material and therefore must be determined experimentally. For steel we found approximately $\eta = 0{,}3$ mm.

2. Plastic Range

While the stress concentration factor (SCF) in the elastic range (i.e. the ESCF) generally can be determined only from the geometrical data of the notched part, in the plastic range the value depends also on the magnitude of the load. As it is well known the SCF decreases with increasing load, whereby the behaviour of the material (stress-strain curve) plays an important influence.

The theoretical treatment of the decrement of the SCF with increasing load is essentially based on the following non-linear stress-strain equation due to H. Neuber

$$\sigma = \frac{E\,\varepsilon}{\sqrt{1 + \left(\frac{E\varepsilon}{\sigma^*}\right)^2}} \tag{14}$$

This equation can be adapted to the real stress-strain curve of a material only if the parameter σ^* in relation to the strain ε is suitably fixed. This fixation follows from the condition that the deformation-work done in uniform tension in the case of the real stress-strain curve and the substituted curve according to eq.(14) are equal.

At first the integral

$$J(\varepsilon) = \int_0^{\varepsilon} \sigma_w \, d\varepsilon \tag{15}$$

is determined by planimetering of the real stress-strain curve. On the other hand the eq.(14) is also integrated

$$\int_0^{\varepsilon} \sigma \, d\varepsilon = \int_0^{\varepsilon} \frac{E\,\varepsilon\, d\varepsilon}{\sqrt{1 + \left(\frac{E\varepsilon}{\sigma^*}\right)^2}} \tag{16}$$

By the condition

$$\int_0^{\varepsilon} \sigma \, d\varepsilon = \int_0^{\varepsilon} \sigma_w \, d\varepsilon = J(\varepsilon) \tag{17}$$

(for any strain ε) one finds the parameter σ^* as a function of ε

$$\sigma^* = \frac{E \cdot J(\varepsilon)}{\sqrt{(E\varepsilon)^2 - 2E \cdot J(\varepsilon)}} \tag{18}$$

Thus by the eqs. (14) and (18) the substitute stress-strain curve is determined. For example, the corresponding curves are plotted for the material St.00.12 in Fig.7A.

From this, one can immediately obtain

$$\frac{\sigma_E}{\sigma^*} = \frac{\sigma_E}{\sigma^*}\left(\frac{\sigma_w}{\sigma^*}\right) \tag{19}$$

$$\sigma^* = \sigma^*\left(\frac{\sigma_w}{\sigma^*}\right) \tag{20}$$

$$\sigma^* = \sigma^*\left(\frac{\sigma_E}{\sigma^*}\right) \tag{21}$$

(see Figs.7B and 7C).
From Fig.7C one can calculate for various values $\sigma_N^* = \text{const}$ the relation

$$\frac{\sigma_E}{\sigma^*} = \frac{\sigma_E}{\sigma^*}\left(\frac{\sigma_N^*}{\sigma^*}\right) \tag{22}$$

shown in Fig.7D.

The theory which is based on eq.(14) yields a relation between the linear maximum stress $\sigma_i/\sigma^* = \alpha \cdot \sigma_N/\sigma^*$ and the non-linear maximum stress σ_{MAX}/σ^* with the non-linear nominal-stress σ_N^*/σ^* entering as a parameter. The result of these rather extensive calculations is shown in Fig.8.

Whereas in the case of pure tension, the non-linear nominal stress is equal to the linear nominal stress, i.e. $\sigma_N^* = \sigma_N$ there exists a difference between the two in bending and in torsion.

In the case of bending for <u>rectangular cross-sectioned bars</u> follows, based on eq.(14)

$$\left.\begin{aligned} \frac{\sigma_N^*}{\sigma^*} &= \frac{m}{\sqrt{m^2+1}} \\ \text{and} \qquad \frac{\sigma_N}{\sigma^*} &= \frac{3}{2}\,\frac{m\sqrt{m^2+1} - \ln\left(\sqrt{m^2+1}+m\right)}{m^2} \end{aligned}\right\} \qquad (23)$$

The relation between σ_N^*/σ^* and σ_N/σ^* is shown in Fig.9.

The Figs. 10 and 11 follow directly from the Figs.8 and 9, and show the relations between σ_{MAX}/σ^* and σ_N^*/σ^* with the ESCF α as a parameter in the case of tension and bending respectively.

By combination of Figs.7B, 7C,7D and 11 the Fig.12 can be drawn from which the real maximum stress can be found as a function of the nominal stress.

For example let us take the case of a notched steel bar (Steel St.00.12) in bending with the ESCF $\alpha = 2{,}0$. Starting from the curve $\sigma_N^* = 16$ kg/mm^2 one finds the intersection-point S_1 with the curve $\alpha = 2{,}0$. Then the belonging values are determined:

$$\frac{\sigma_N^*}{\sigma^*} = 0{,}36 \qquad \frac{\sigma_w}{\sigma^*} = 0{,}57 \qquad \sigma^* = 132 \text{ kg/mm}^2$$

From Fig.9 one can find with $\sigma_N^*/\sigma^* = 0{,}36$ the value $\sigma_N/\sigma^* = 0{,}37$ and hence $\sigma_N = 48{,}9$ kg/mm^2. For this nominal stress one obtains the SCF

$$\frac{\sigma_{MAX}}{\sigma_N} = \frac{\sigma_W}{\sigma_N} = 1{,}54$$

This worked example is indicated by arrows in Fig.12.

The method mentioned above was applied to four different materials (steel St.00.12, steel St.00.21, pure Aluminum, Aluminum alloy "Velodur"), for which the stress-strain curves had been exactly determined (cf. Figs. 12A - D), and the dependence of the SCF from the nominal stress for various ESCF's in tension and bending evaluated. The results are laid down in Figs. 13 - 16.

The Figs. 29 - 32 show that the theoretical results are in satisfactory agreement with the experimental results (in the theoretical calculation the experimental ESCF's had been taken).

III. EXPERIMENTAL PART

1. Materials Used

The materials used for the tests are listed in table 1. There are also tabulated the mechanical and chemical properties.
The stress-strain curves of these materials determined by us are shown in Figs. 22A - D.

2. Specimen Types

The tests were carried out with strips, the shape and size of which are shown in Figs. 23A - C. The specimens with a pair of symmetrical semicircular notches and with a central hole were used for the tension tests. The bending tests were made with single-notched bars.

3. Testing Equipment

The tension specimens were loaded in the Amsler testing-machine of the type 2 ZD 182 and in the Losenhausen testing-machine UHS 60. The specimens with a central hole in the case $a/\rho = 0{,}1$ were loaded with weights. Fig. 17 shows a specimen clamped in the testing-machine UHS 60. The loading fixture can be seen in Fig.20.

The bending tests were made in the Losenhausen testing-machine UHS 20. The equipment used for these tests is shown in Figs. 18 and 21.

4. Measuring Equipment and Test Procedure

4.1. Electrical Strain Measurements

For each tests because of the great number of measuring points the following three instruments had been used:

Philips measuring bridge PR 9300 in connection with Philips balancing and switching units FE 245 (for 10 measuring points)

Hottinger measuring bridge KWS II in connection with Philips balancing and switching units FE 245 (for 10 measuring points)

Philips measuring bridge PR 9200 (for the other measuring points).

The assemblage of the measuring instruments is shown in Fig. 19.

The following strain gages and binding material are used:

10/120 FB1 active gage length 10 mm
6/120 FB1 active gage length 6 mm
3/120 FB1 active gage length 3 mm

Hottinger binding material "H" and rapid binding-material "X 57".

For the bending tests the steel St.00.21 had been used. Tension specimens with a central hole were of the materials steel St.00.12, pure Aluminum and Aluminum alloy "Velodur", tension specimens containing a pair of symmetrical semi-circular notches were of the materials steel St.00.12, Special steel DN 36, pure Aluminum and Aluminum alloy "Velodur".

Two specimens of the same kind were prepared from each material. For each specimen 24 - 28 strain gages were used;

the strain gages were attached on both sides of the specimens in the same arrangement which is shown in Fig.20.

The load were applied to a maximum strain in the notch of 1,2 - 1,5 %. In the plastic range measurements were taken at 5 - 7 load steps, in the plastic range at 8 - 10 load steps.

4.2. Photoelastic Measurements by Means of the Stress-Coat Method

For the tension tests with "Velodur"-specimens as given in Fig. 23A, measurements by means of the photoelastic stress-coat method were made in addition to the strain measurements with electrical strain gages. In this method a thin plate of photoelastic material (Epoxy resin Araldite B, manufactured by CIBA-Company Basel) is stuck on the metal and the loaded strip is observed in monochromatic polarized light, which is reflected by the metal surface (see Fig.24).

From the isochromatic patterns immediately follow the edge-stresses in the Araldite layer and by means of the stress-strain curve of Araldite one obtains the strain, which is equal to the strain of the tested metal. By means of the stress-strain curve of the metal one obtains finally the edge-stresses in the metal strip. The SCF can then be calculated from the stress in the notch. This method is mainly suitable for investigations in the plastic range, for in this case the occuring deformations provide a fringe order which is more than sufficient for a proper analysis.

The Araldite plates had been casted in suitable thickness (for "Velodur" 2 mm) from the Araldite B "Gießharz" with hardener No. 901 which is mixed in the proportion 10:3.

After a thorough cleaning of the metal specimen, the Araldite plate had been stuck on with the cold-hardening cementing-material Araldite 103 with hardener 951, mixing proportion 100:7,5 (time of hardening 48 hours at room-temperature) which guarantees the necessary adhesive strength. To obtain a very exact analysis, on both sides of the metal specimen in this way Araldite plates were stuck and measurements were taken on both sides. The testing-equipment is shown in Fig.24A.

The isochromatic patterns at various loads were photographed (examples see Fig.25).

5. Analysis of the Measurements and Results

5.1. Electrical Strain Measurements

Investigations with notched specimens generally are carried out without consideration of the strains on the transverse axis of the specimen. For a correct determination of the stress distribution over the minimum section however the knowledge of the strains in both directions is indispensable. Therefore in our tests we measured the strains in the longitudinal and transverse axis of the specimens. Further in the analysis we took in account the transverse sensitivy of the electrical strain gages in a suitable way (cf. [5]). The notch stress in the elastic and plastic range follows from the strain in the notch

$$\varepsilon = \frac{1}{k} \frac{\Delta R}{R} \qquad (24)$$

(whereby $\Delta R/R$ means the change of resistance of the strain gage and k a factor)

and the stress-strain curve of the material tested.

The ESCF's obtained in this way for the investigated notch-shapes of various sizes are shown in Figs. 26 - 28. They are mean values of tests with various materials (two tests for each specimen shape and material). In Fig. 28 also photoelastic measurements by Leven and Frocht [6] are plotted.

In the plastic range the SCF is not only dependent on the notch-shape, but also on the material and the magnitude of the load. The SCF as a function of the nominal stress for the used materials and specimen shapes is shown in the Figs. 29 - 32. Certain anomalies were observed with Aluminum, which can be explained by grain influences and the special yield-behaviour of the pure Aluminum.

The stresses over the minimum section in the elastic range had been calculated from the measured strains ε_x and ε_y according to

$$\left.\begin{aligned} \sigma_x &= \frac{E}{1-\nu^2}\left(\varepsilon_x + \nu\,\varepsilon_y\right) \\ \sigma_y &= \frac{E}{1-\nu^2}\left(\varepsilon_y + \nu\,\varepsilon_x\right) \end{aligned}\right\} \qquad (25)$$

Herewith the mean values from the measured strains on both sides of the specimen are taken. The stress distributions over the minimum section in the elastic range for various notch sizes are drawn in Figs. 33 - 37. They are the mean values of the tests with various materials (two tests for each specimen-shape and material).
In the plastic range the relation (25) is no more valid. Therefore only the measured strains are delivered (see Figs. 38 - 49).

In the Figs. 26 - 28 also the scattering of the test results is shown. The most exact results in the elastic range were

obtained with the material "Velodur", whereas pure Aluminum showed the greatest scattering. The exactness of the strain gages is 1,5 %, of the elastic constants (E and G) is about 4 %, and for the indication of the testing machine is 1 %.

5.2. Photoelastic Stress-Coat Method

The basic equation of photoelasticity

$$\tau_H = \frac{S}{2} \frac{\delta}{d^*} \tag{26}$$

yields a relation between the principal shear stress τ_H and the order of isochromatics δ in a model of photoelastic material (Araldite). d^* means the "effective" thickness of the model, which in the stress-coat method because of the reflection (twice the path of light in the model) is equal to twice the thickness of the Araldite layer. S is the photoelastic constant which has to be determined by a calibration tests (we found S = 10,6 kg/cm order).

Along the non-loaded edge there is $\sigma_n = 0$ (stress perpendicular to the edge) and therefore

$$\tau_H = \frac{\sigma_t}{2} \tag{27}$$

whereby σ_t means the tangential edge stress. With restriction to an analysis of the isochromatic pattern along the edge it follows from eqs.(26) and (27) the edge-stress in the Araldite layer (dashed letters concern the Araldite)

$$\sigma_n' = 0 \qquad \sigma_t' = \frac{S\delta}{d^*} = \frac{S\delta}{2d'} \tag{28}$$

The Araldite plate, which is stuck on the metal specimen is forced to take the strain of the loaded metal. The load is transferred from the metal specimen to the Araldite layer by means of shear stresses τ through an area near the end of the layer (see Fig.24B).

In the case of equality of the Poisson's ratios ($\frac{1}{\nu} = \frac{1}{\nu'}$) of both materials, in the elastic range shear stresses occur at no other places of the cementing layer. By means of strain measurements the following values had been determined:

for Araldite $\nu' = 0{,}38$; for Velodur $\nu = 0{,}30$

Hence the condition of equality of the Poisson's ratios is approximately fulfilled. At the edge eq.(28) is valid for Araldite.

From Hooke's law and with eq. (28) follow the edge-strains of the Araldite plate and the metal in the elastic range

$$\varepsilon_t' = \frac{\sigma_t'}{E'} \qquad \varepsilon_t = \frac{\sigma_t}{E} \tag{29}$$

From the condition $\varepsilon_t = \varepsilon_t'$ with $\nu = \nu'$ one obtains

$$\sigma_t = \frac{E}{E'}\sigma_t' = \frac{E}{E'}\frac{S\delta}{2d'} \tag{30}$$

The metal carries the fraction of the total force P introduced into the strip

$$P_o = \frac{P}{1 + 2\frac{E'}{E}\frac{d'}{d}} \tag{31}$$

Therefore the nominal stress in the metal is

$$\sigma_N = \frac{1}{1 + 2\frac{E'}{E}\frac{d'}{d}} \cdot \frac{P}{F} \qquad (32)$$

whereby F means the area of the minimum cross section of the metal.

From eqs.(30) and (32) it follows the ESCF

$$\alpha = \frac{\sigma_{t\,MAX}}{\sigma_N} = \left(\frac{E}{E'} + 2\frac{d'}{d}\right)\frac{F}{P}\,\frac{S\,\delta_{MAX}}{2d'} \qquad (33)$$

Because of the small strains in the elastic range, there occur only a few fringe orders (the thickness of the Araldite layer was chosen in such a way that about two fringe orders occur at the metal's yield stress in the notch), and therefore an exact determination of the isochromatic orders was only possible by means of compensating.

When greater loads are applied, the metal is already plastic, but the Araldite largely follows the linear stress-strain relation. The now appearing inequality of the transverse strain in Araldite and in the metal is compensated by additional shear stresses, which occur in the cementing layer. Immediately at the edge however eq.(28) will be valid with good approximation. In the analysis one proceeds as follows (see Fig.50, in which the relation (28) is plotted for the used thickness of the Araldite plate and also the stress-strain curves of Araldite and Velodur are shown).

From the isochromatic order δ at the edge first the edge-stress in Araldite is determined, which yields the strain

and finally the edge-stress in the metal (Velodur). By evaluating the nominal stress in the metal by eq.(8), which is approximately valid, one obtains the SCF in the plastic range for various values of σ_N (shown in Fig. 52). The experimentally determined relation between the fringe order δ in the notch and the applied load P is plotted in Fig. 51. In a similar way one obtains the curve of the tangential edge-stress σ_t (see Fig. 35).

IV. BIBLIOGRAPHY

[1]	H. Neuber	Kerbspannungslehre 2.Auflage Berlin 1958
[2]	Ch. B. Ling	Journal Appl. Mechanics Vol. 14 (1947) p. 275
[3]	M. Isida	Trans.Jap. Soc. Mech. Eng. Vo. 19 (1953) No. 83, p.5
[4]	R.C.J. Howland	Phil. Trans. Roy. Soc., London Vol. A 229 (1929) p.49
[5]	K. Fink	Grundlagen und Anwendungen des Dehnungsmeßstreifens Düsseldorf 1952
[6]	M. M. Leven M. M. Frocht	Journal Appl. Mechanics Vol. 19 (1952) p.560

V. TABLES AND ILLUSTRATIONS

	St.0012	St.0021	Al	Velodur	Special steel DN 36
Tensile strength (kg/mm^2)	36,2..... 39,3	45,9.... 46,1	7,51..... 7,80	52,7..... 57,8	47,4..... 51,3
Yield point (kg/mm^2)	23,7..... 25,6				
$\sigma_{0,1}$ - Limit (kg/mm^2)			2,5..... 3,0	39,7..... 47,4	21,4..... 22,8
Average Young's modulus (kg/mm^2)	$2,147 \cdot 10^4$	$2,072 \cdot 10^4$	$0,708 \cdot 10^4$	$0,720 \cdot 10^4$	$1,477 \cdot 10^4$
Average shear modulus (kg/mm^2)	$0,806 \cdot 10^4$	$0,817 \cdot 10^4$	$0,272 \cdot 10^4$	$0,273 \cdot 10^4$	$0,582 \cdot 10^4$
chemical composition			Impurities (Si,Fe,Ti, Cu,Zn) < 05 %	Cu 2,0 % Mg 2,5 % Mn 0,1 % Zn 6,5 % annealed at 460°C quenched in water 10 hours age-hardened at 125°C	C 0,03 % Si 0,22 % Mn 0,36 % P 0,009 % S 0,004 % Ni 36,3 % V,Mo traces

Table 1: Materials used

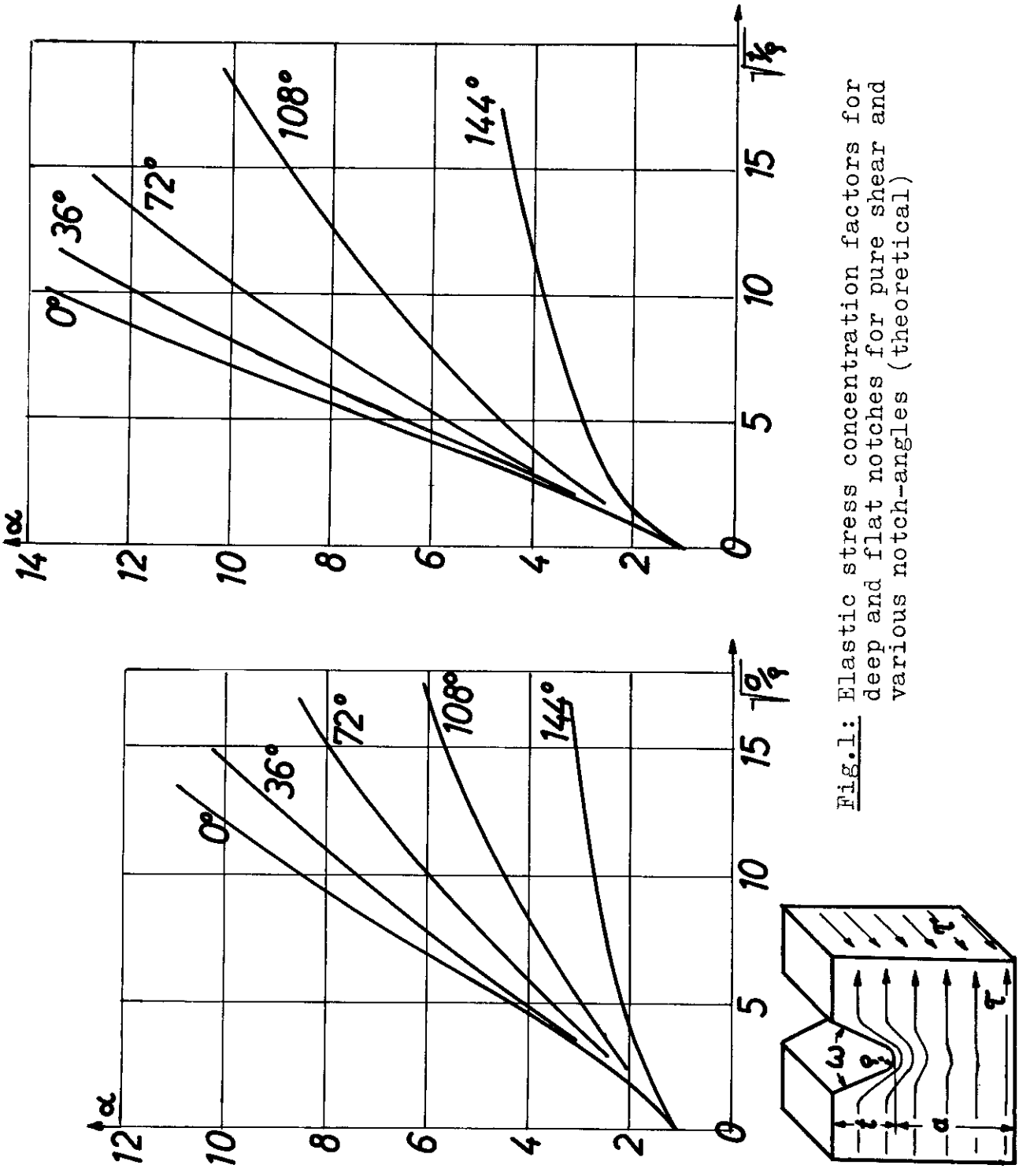

Fig.1: Elastic stress concentration factors for deep and flat notches for pure shear and various notch-angles (theoretical)

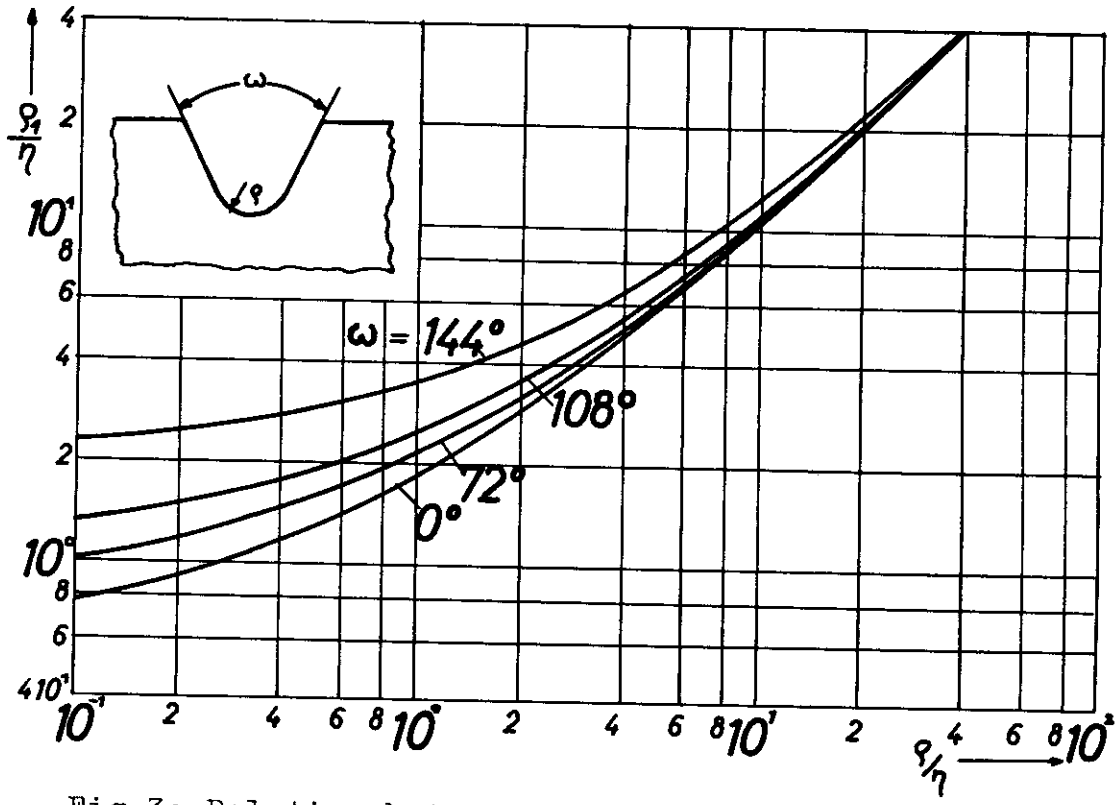

Fig.3: Relation between ρ_1 and ρ for various notch-angles ω in the case of pure shearing

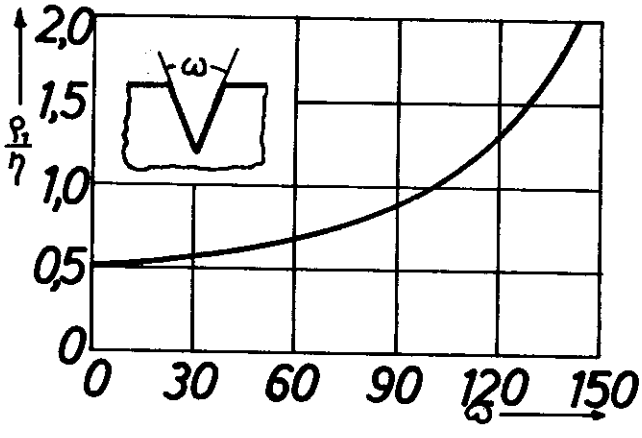

Fig.5: ρ_1 vs. ω for V-shaped notches in shearing

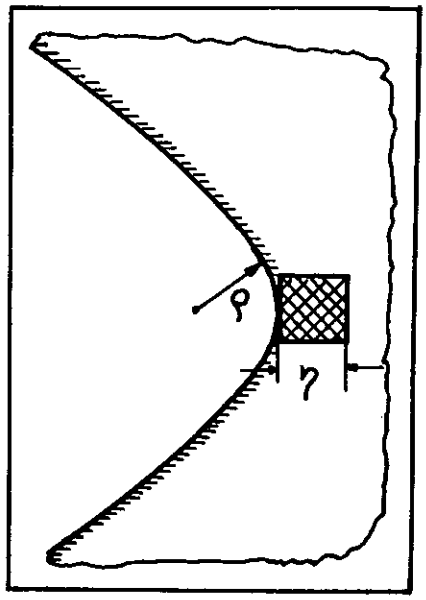

Fig.2: Meaning of the material constant η in the theory of V-shaped notches

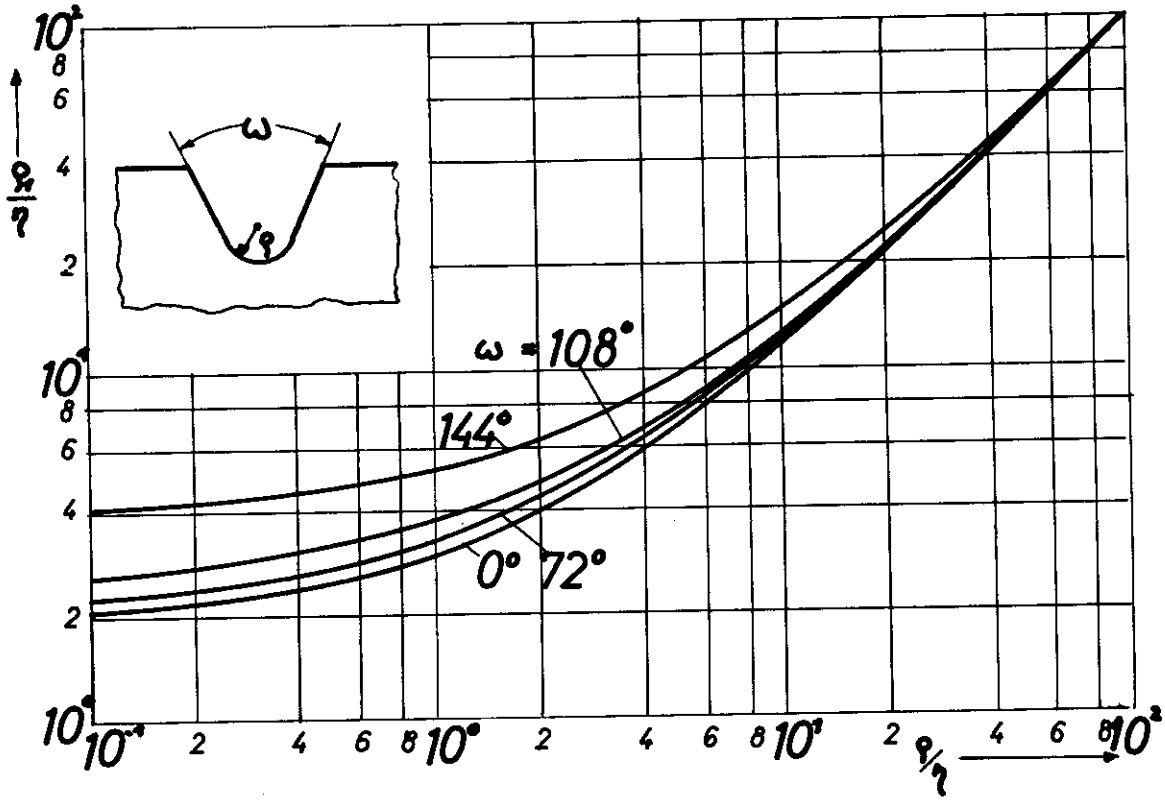

Fig.4: Relation between ρ_1 and ρ for various notch-angles ω in tension

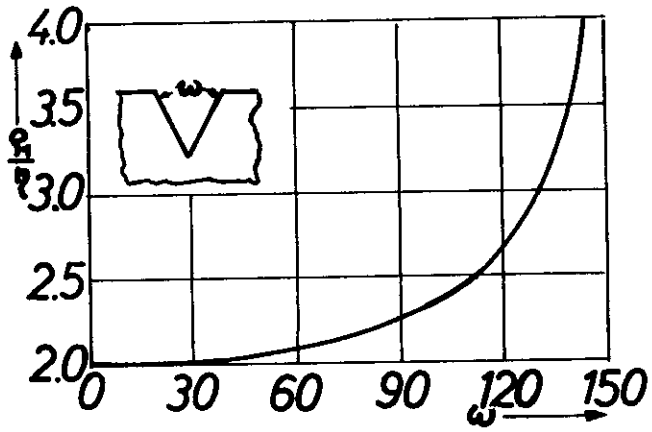

Fig.6: ρ_1 vs. ω for V-shaped notches in tension

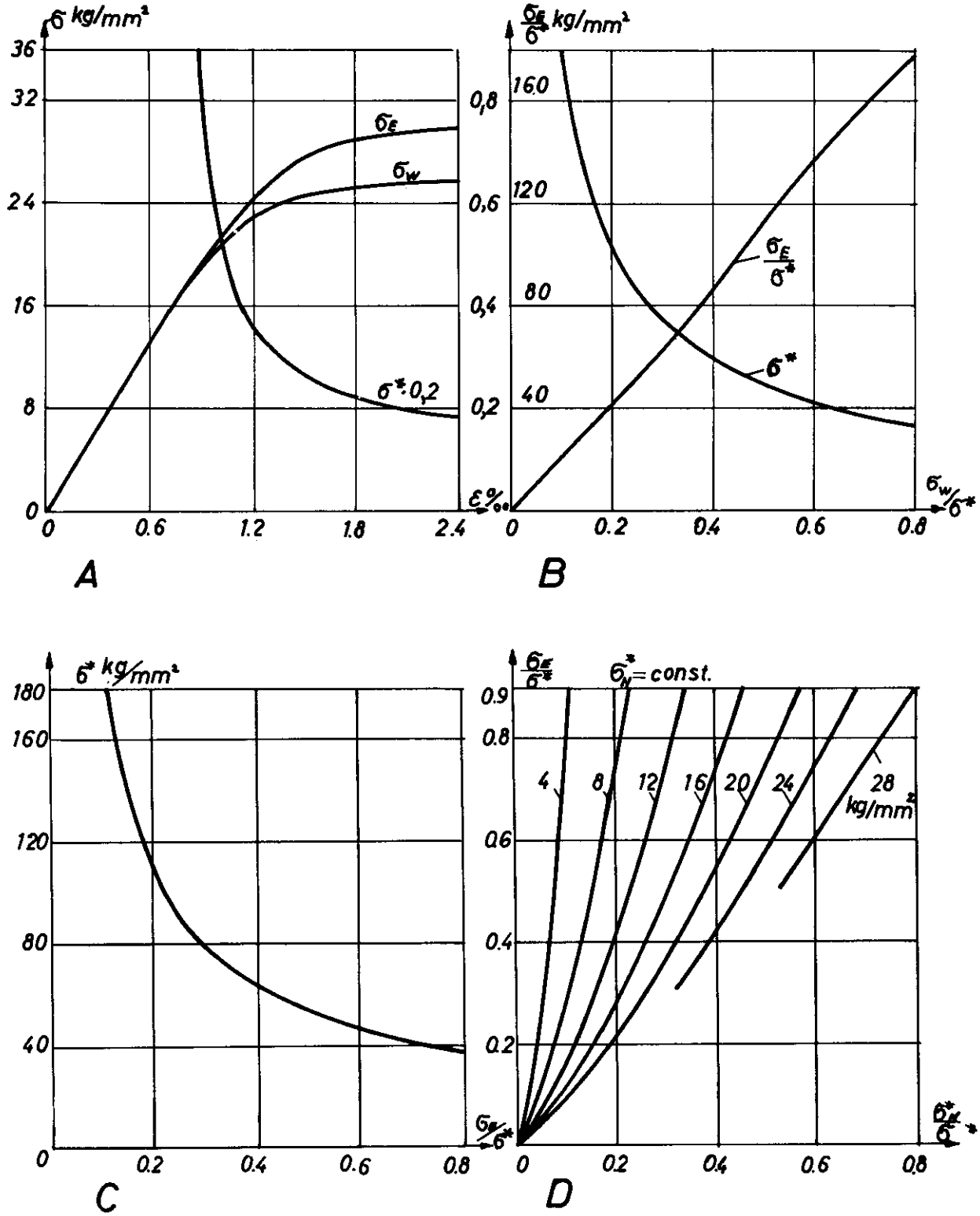

Fig.7: Diagrams for the theoretical determination of the SCF in the plastic range for steel St.00.12

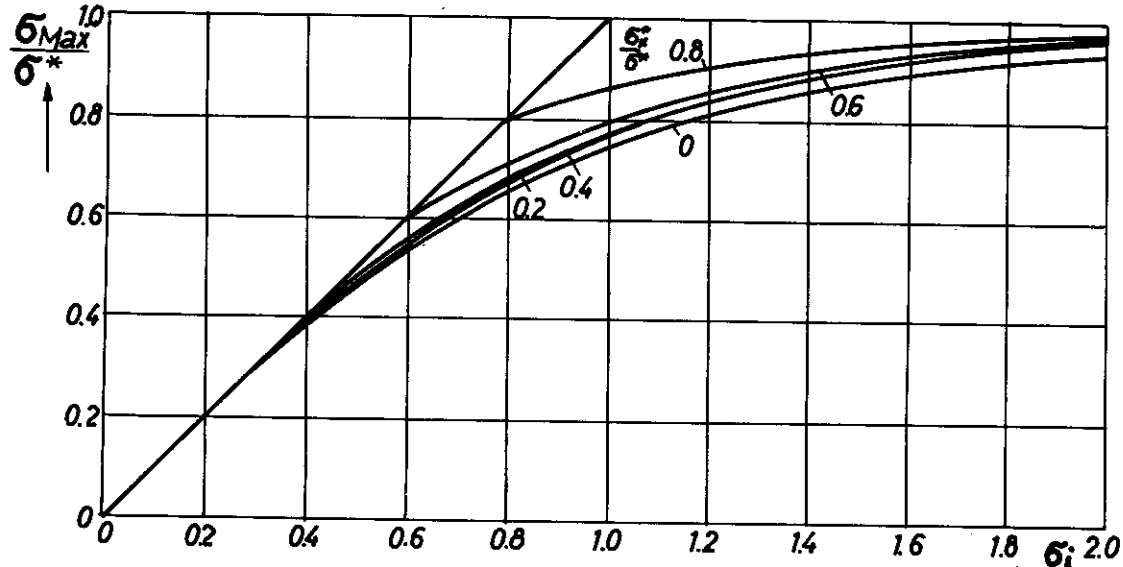

Fig.8: Relation between σ_{MAX}/σ^* and σ_i/σ^* for various σ_N^*/σ^*

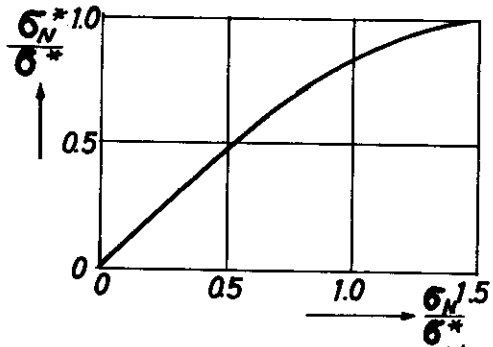

Fig.9: Relation between σ_N^*/σ^* and σ_N/σ^* for a rectangular cross section

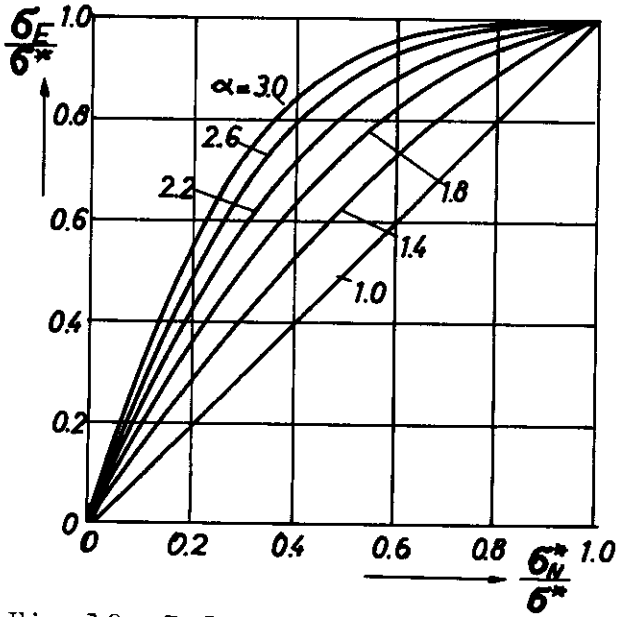

Fig.10: Relation between σ_E/σ^* and σ_N^*/σ^* for various ESCF's in tension

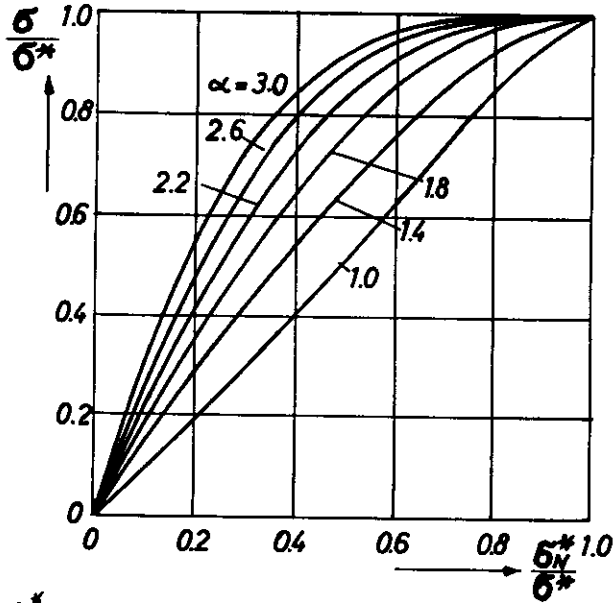

Fig.11: Relation between σ_E/σ^* and σ_N^*/σ^* for various ESCF's in bending

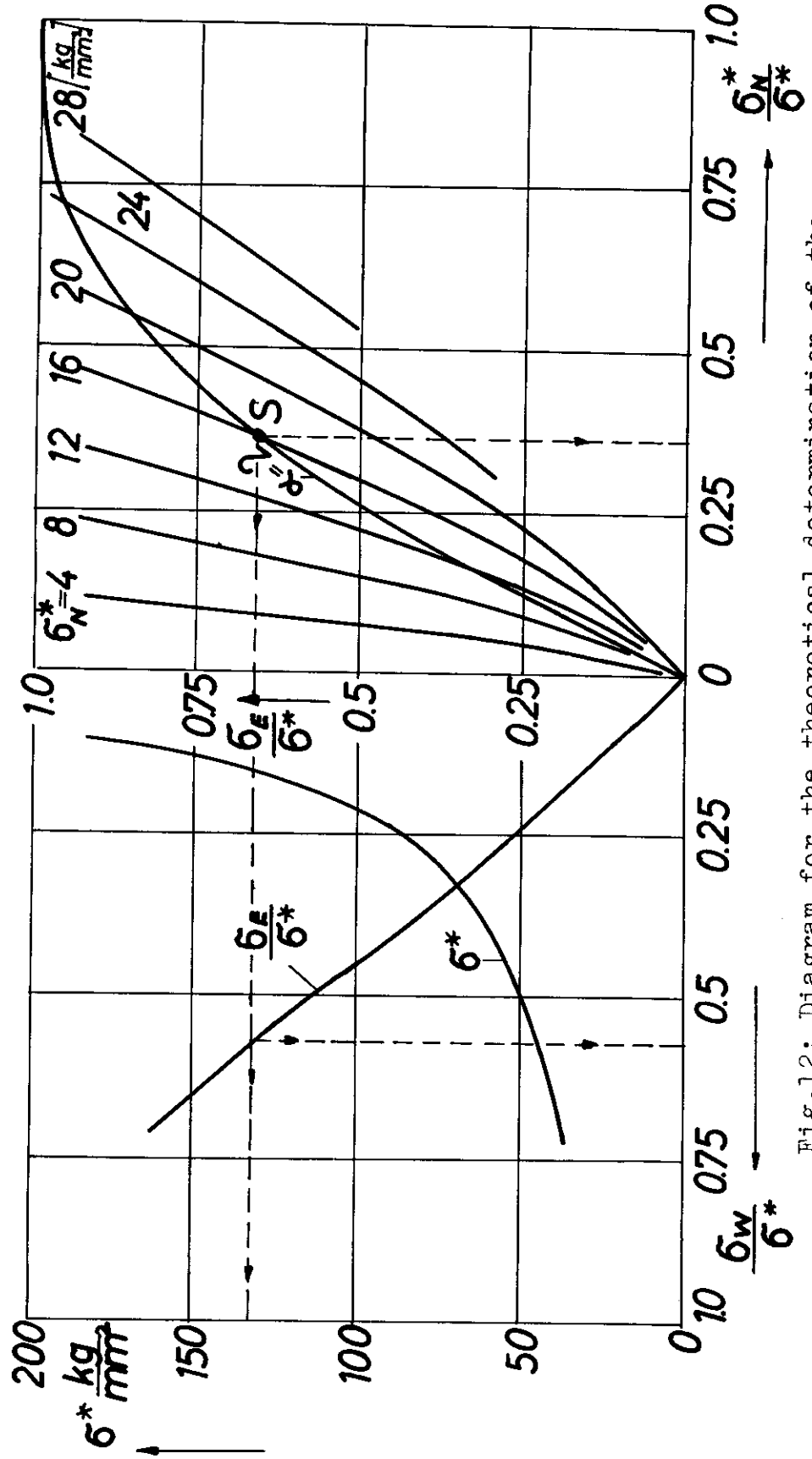

Fig.12: Diagram for the theoretical determination of the notch stress in the plastic range for bending (material St.00.12)

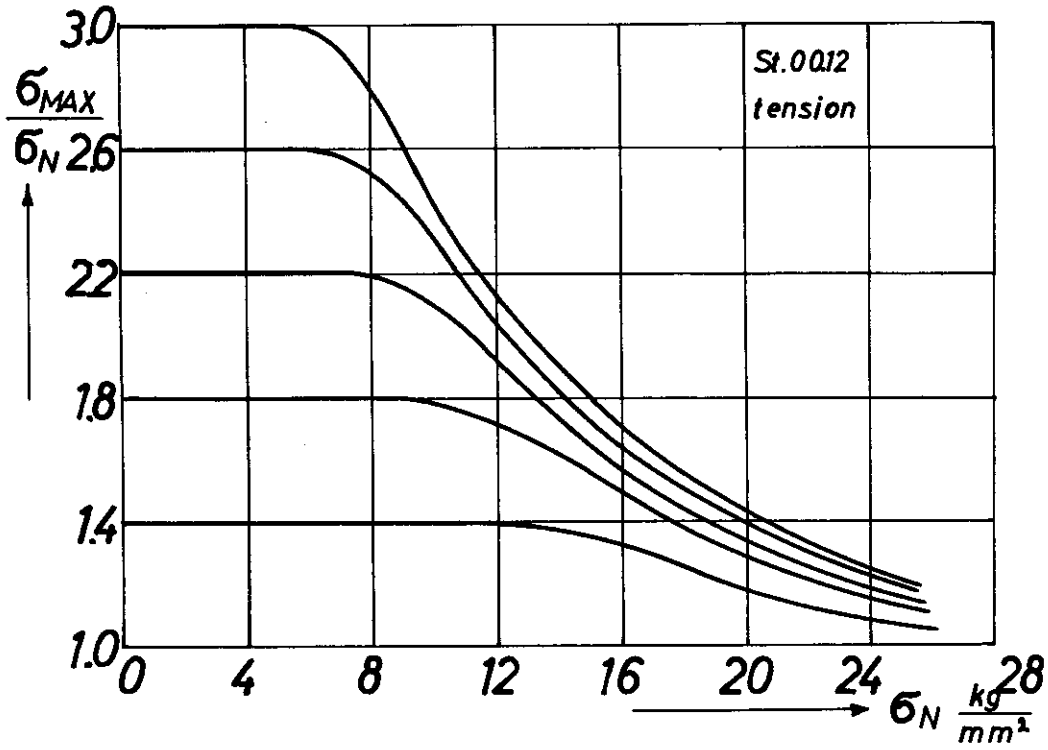

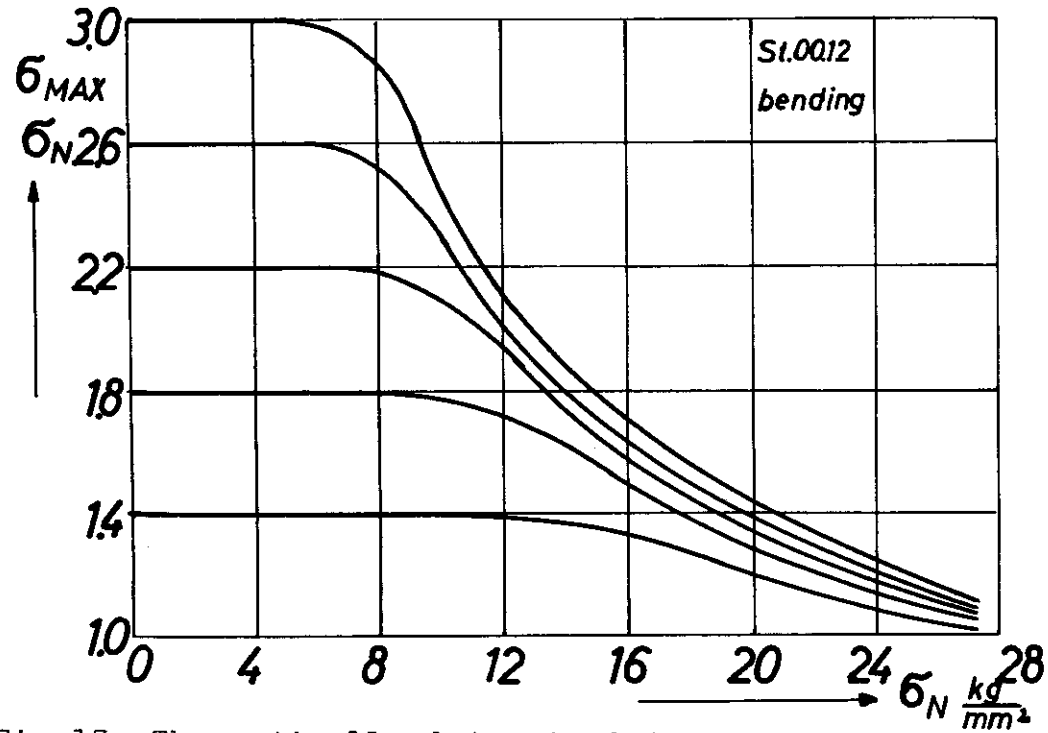

Fig.13: Theoretically determined dependence of the SCF from the nominal stress for tension and bending (material St.00.12)

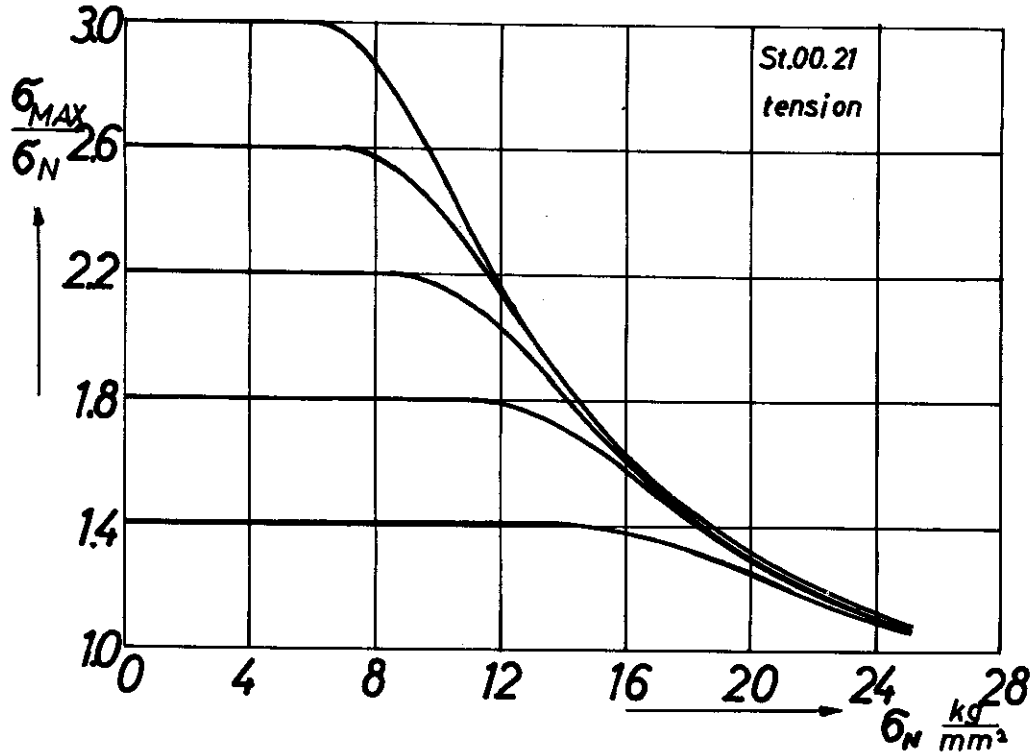

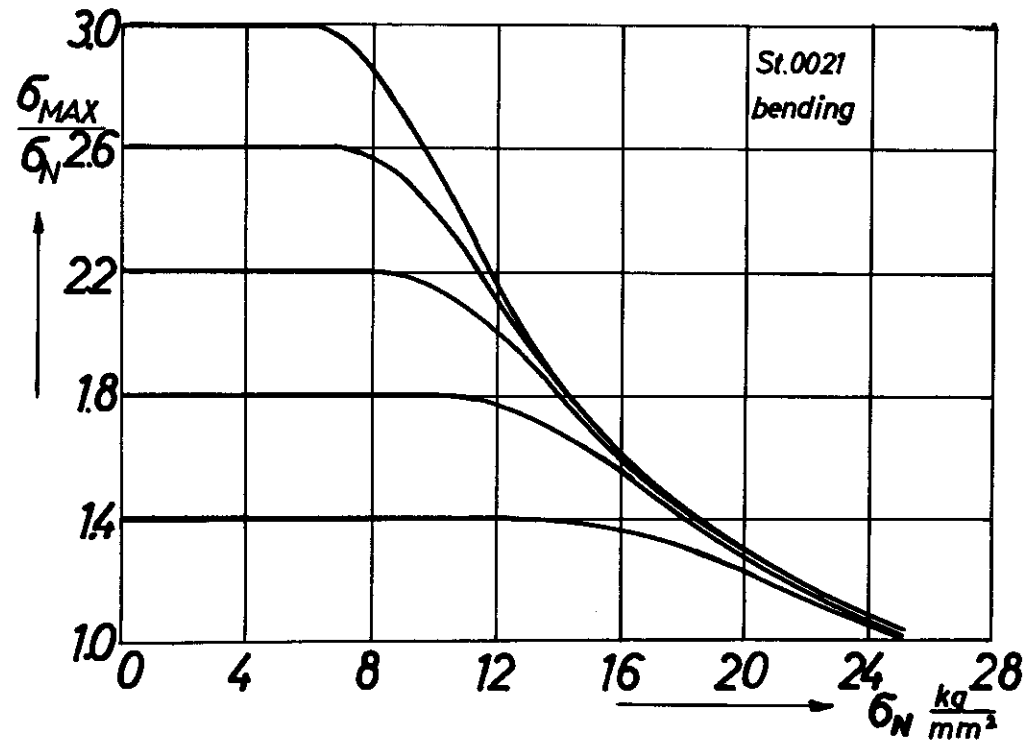

Fig.14: Theoretically determined dependence of the SCF from the nominal stress for tension and bending (material St.00.21)

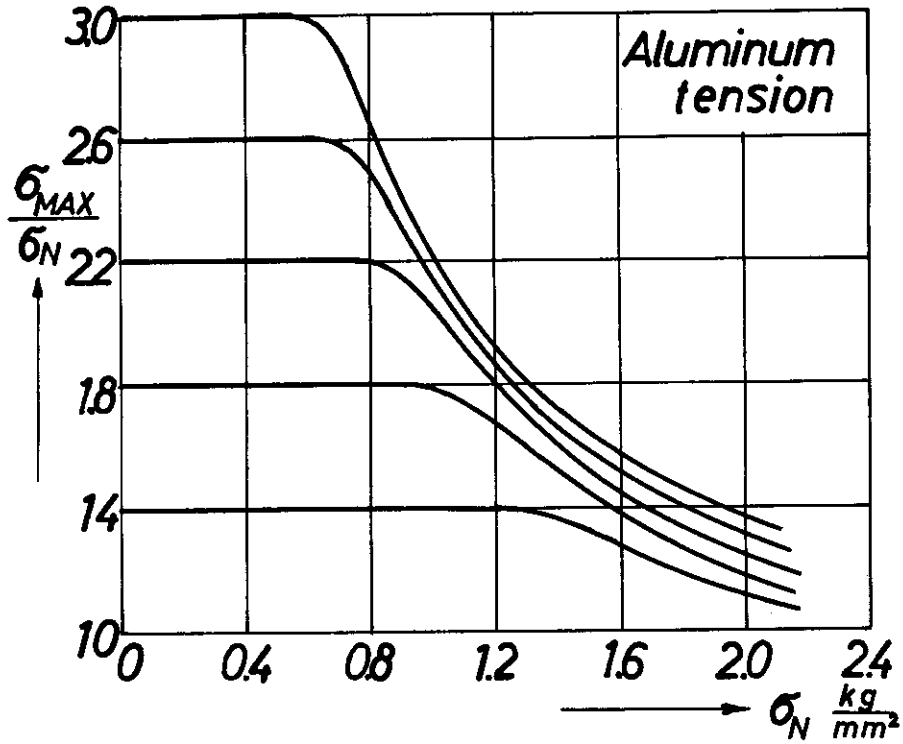

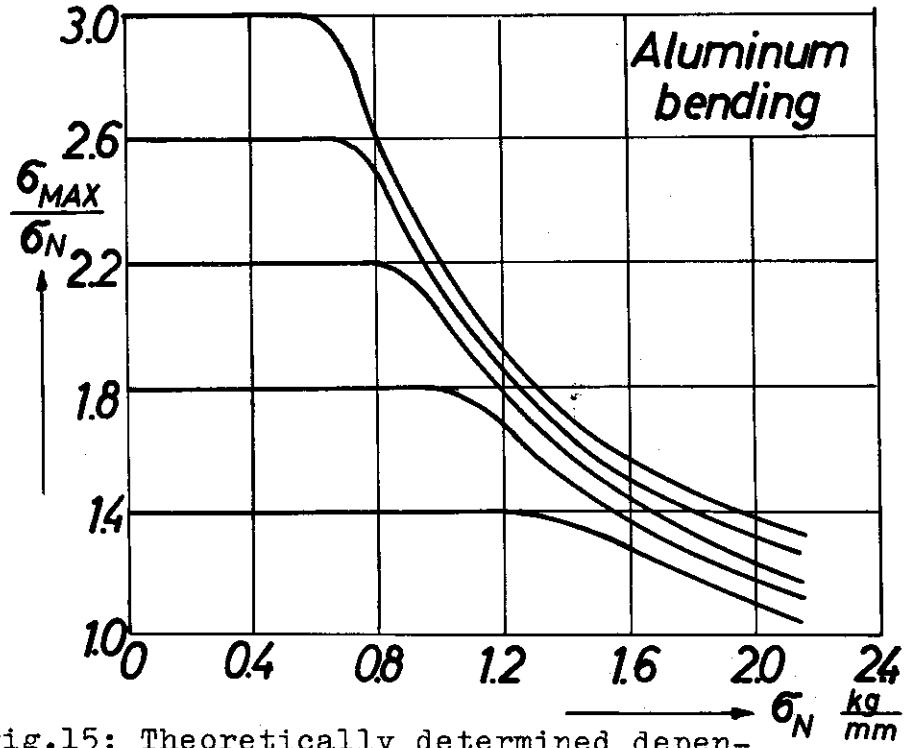

Fig.15: Theoretically determined dependence of the SCF from the nominal stress for tension and bending (material Aluminum)

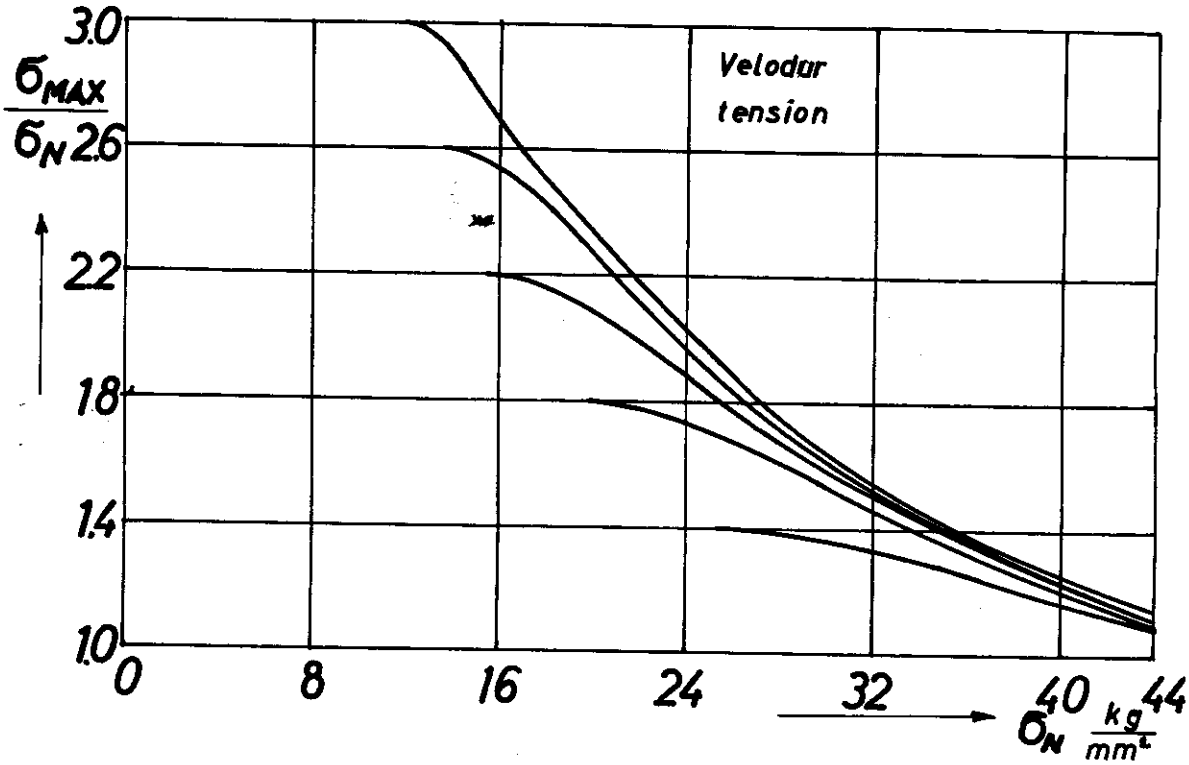

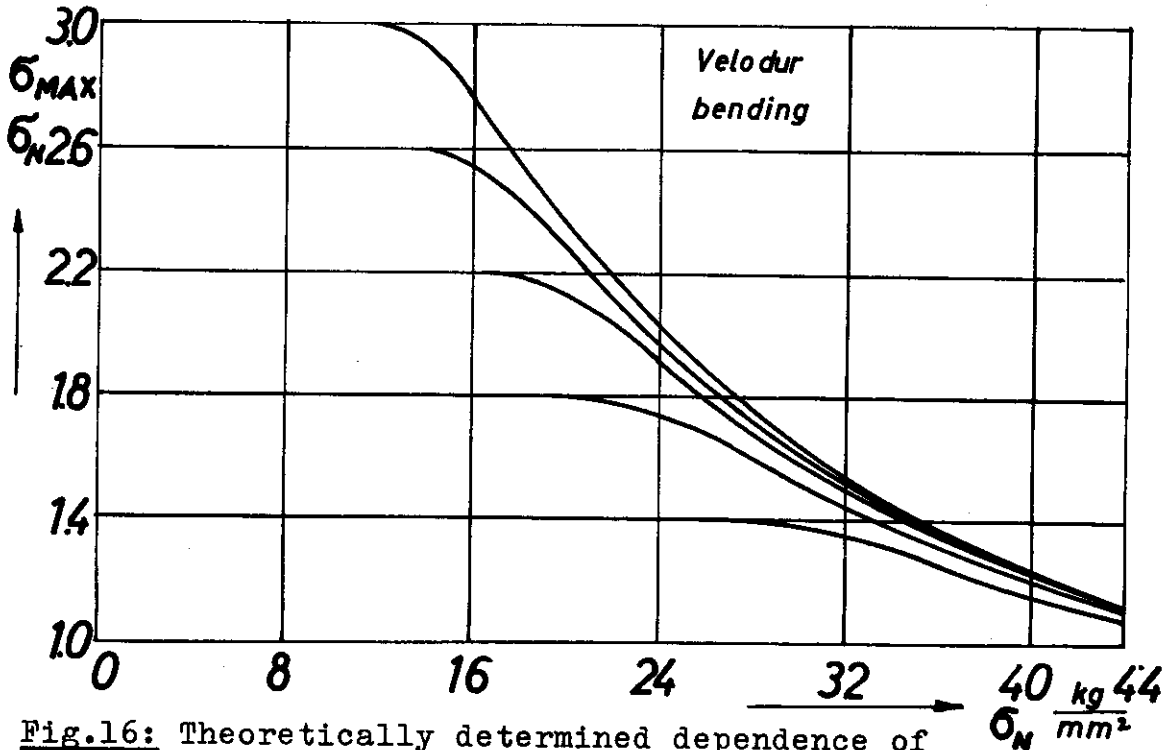

Fig.16: Theoretically determined dependence of the SCF from the nominal stress for tension and bending (material "Velodur")

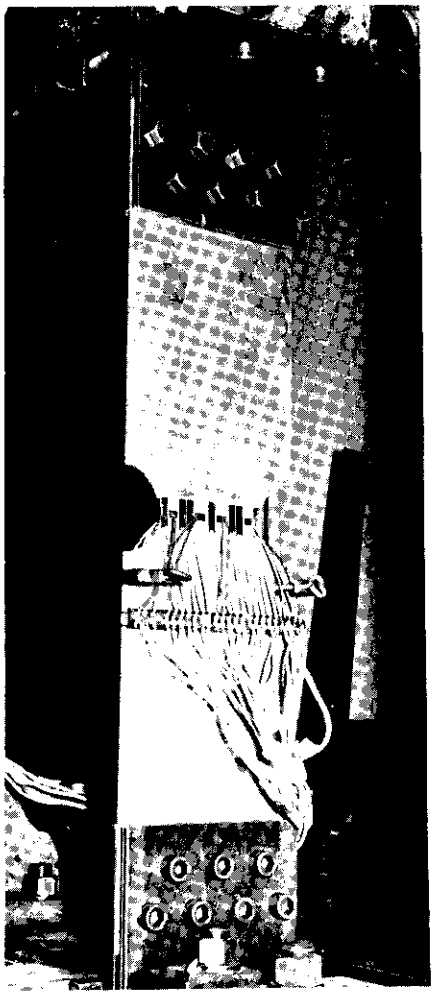

Fig.17: Clamped tension specimen

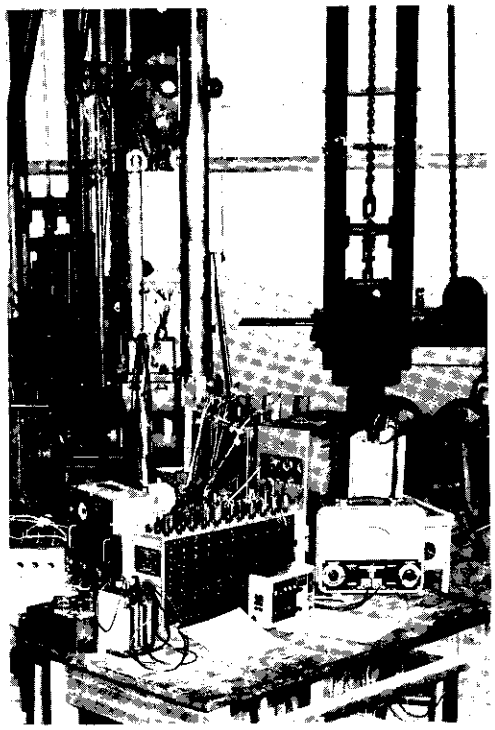

Fig.19: Loading and measuring equipment

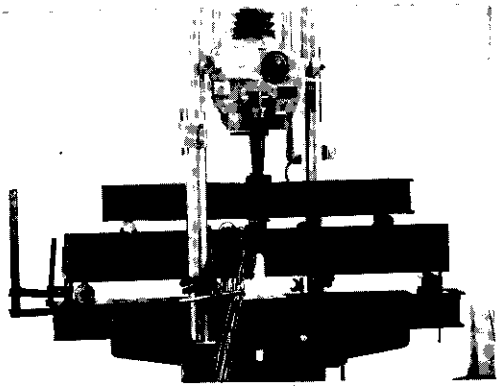

Fig.18: Equipment for bending tests

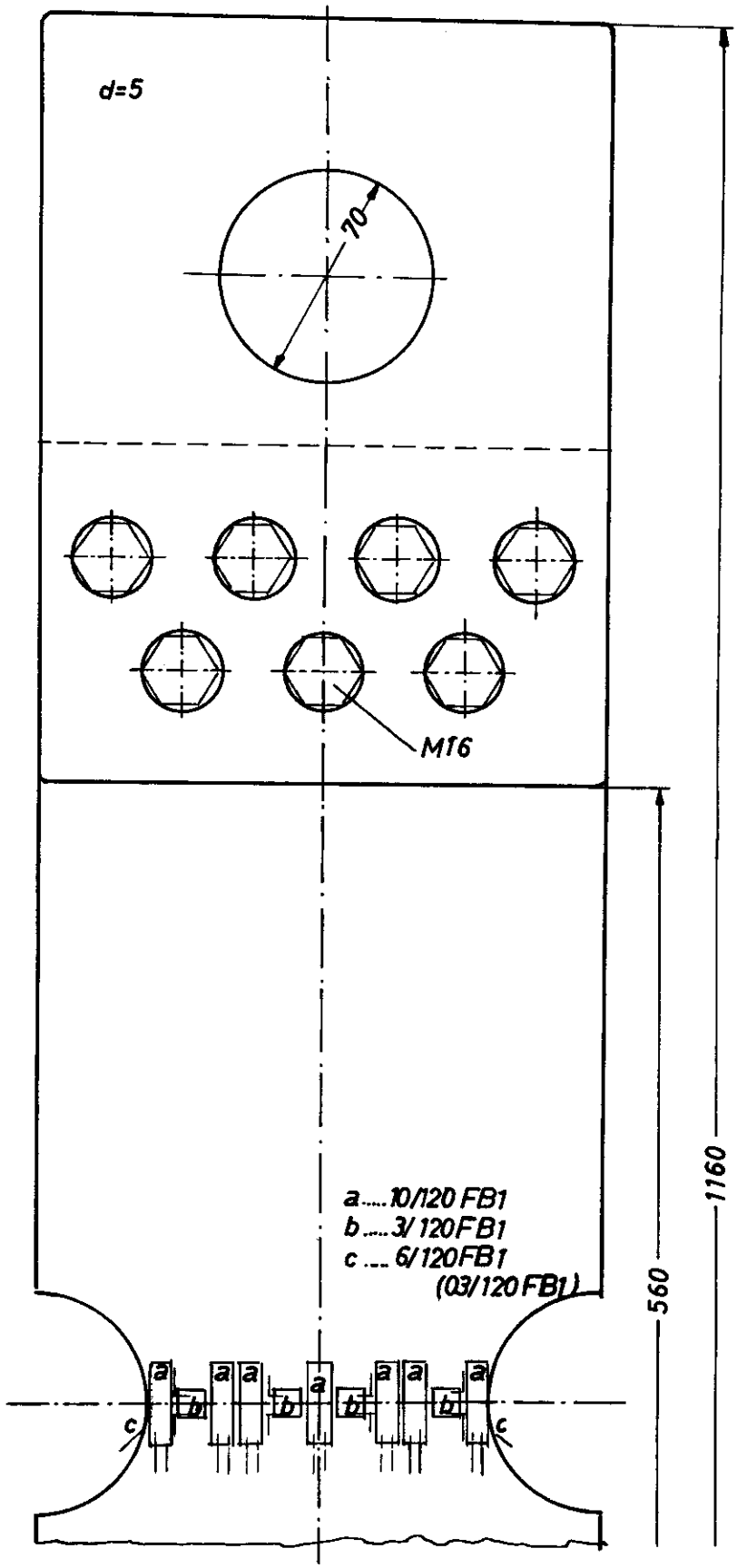

Fig.20: Tension specimen with strain gages

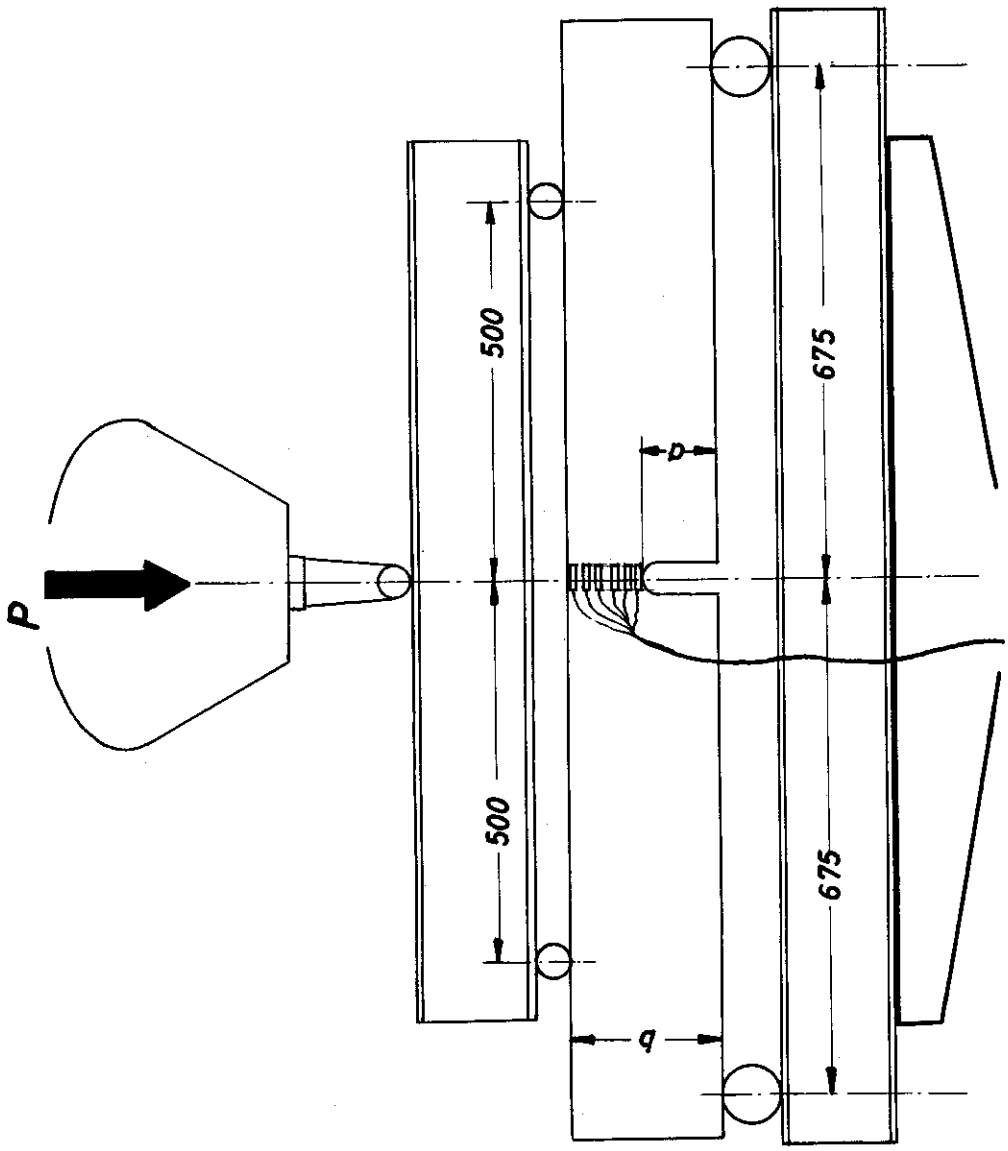

Fig.21: Loading equipment for bending tests (schematically)

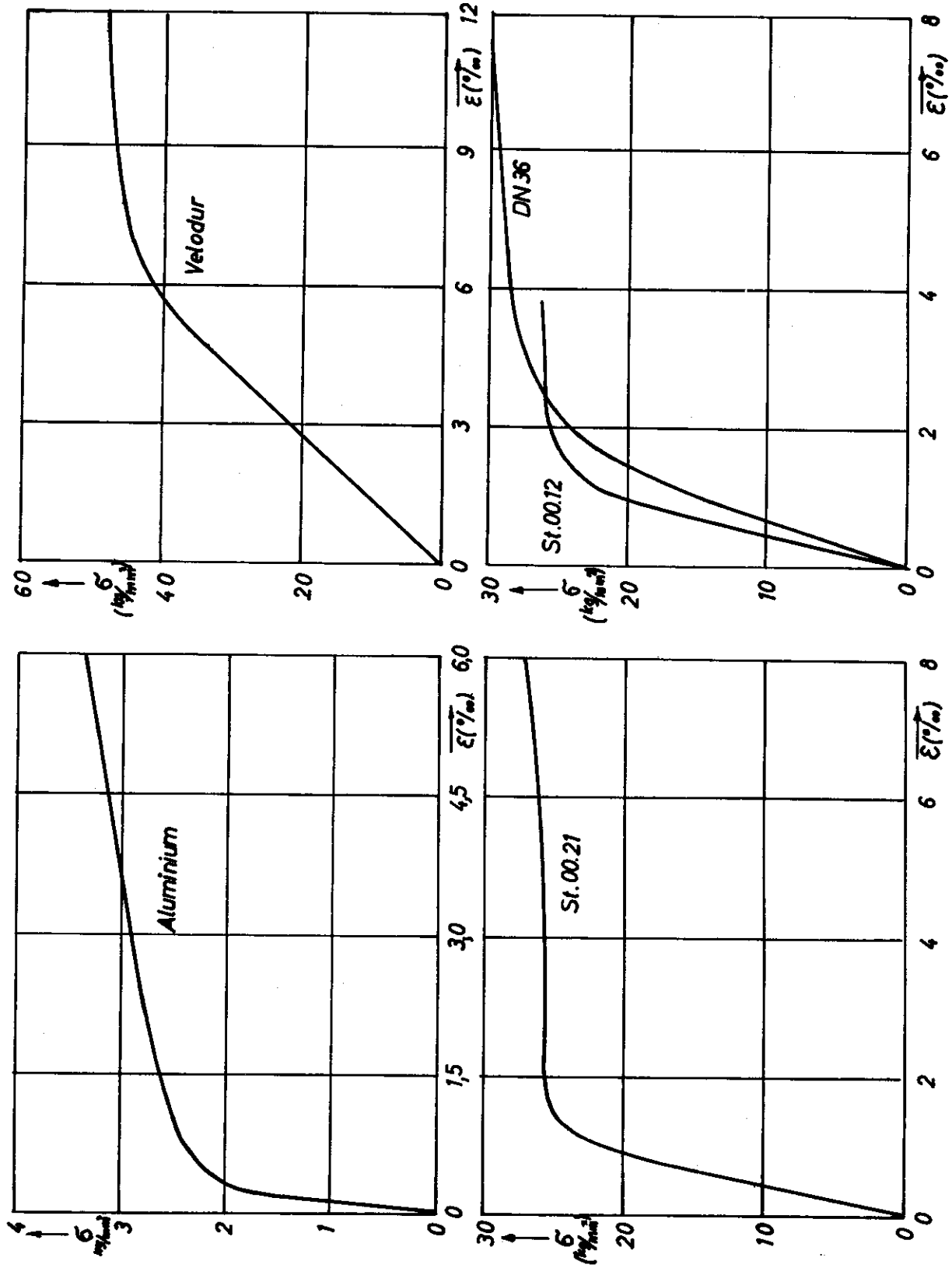

Fig.22: Stress-strain curves for the materials used

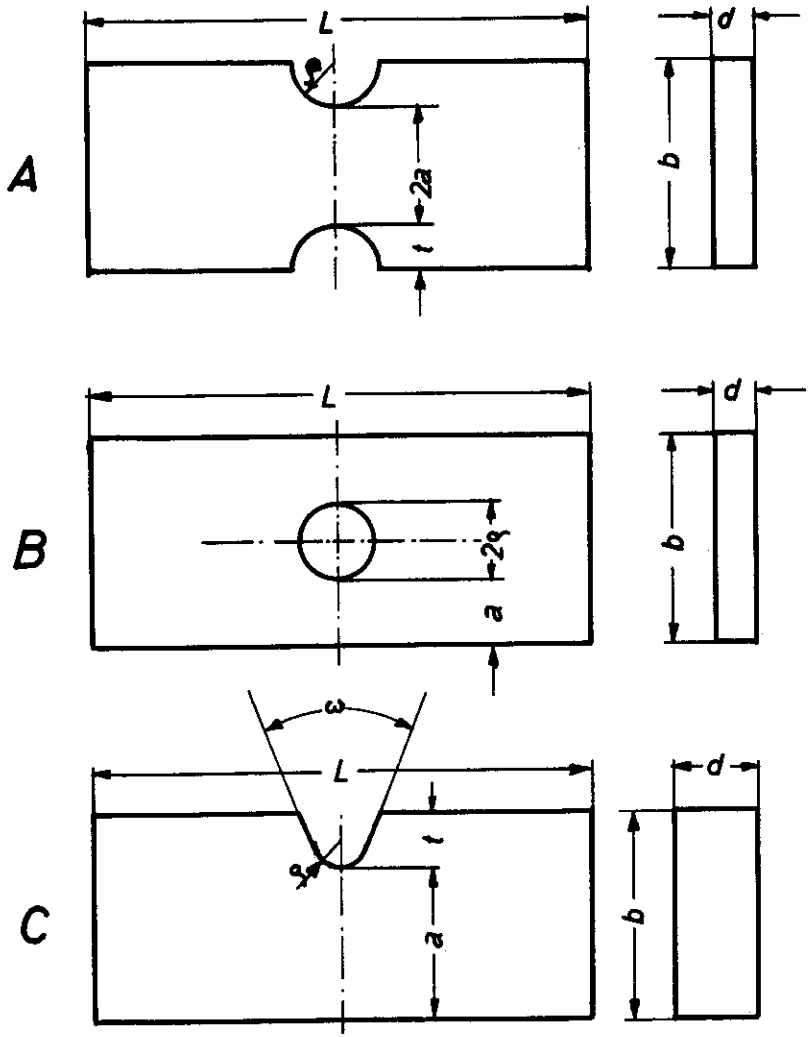

a/ϱ	a	t	ϱ	d	b	L
1	50	50	50	50	200	800
1,5	60	40	40	5	200	800
2	66	33	33	5	200	800
3	75	25	25	5	200	800

a/ϱ	a	t	ϱ	d	b	L
01	9	—	91	5	200	2500
1	50	—	50	5	200	800
15	60	—	40	5	200	800
2	67	—	33	5	200	800
3	75	—	25	5	200	800

a/ϱ	ω	a	t	ϱ	d	b	L
5	0	100	100	20	30	200	1500
	50	100	100	20	30	200	1500
	90	100	100	20	30	200	1500
	150	100	100	20	30	200	1500

Fig.23: Shapes and dimensions (measured in mm) of the specimens used

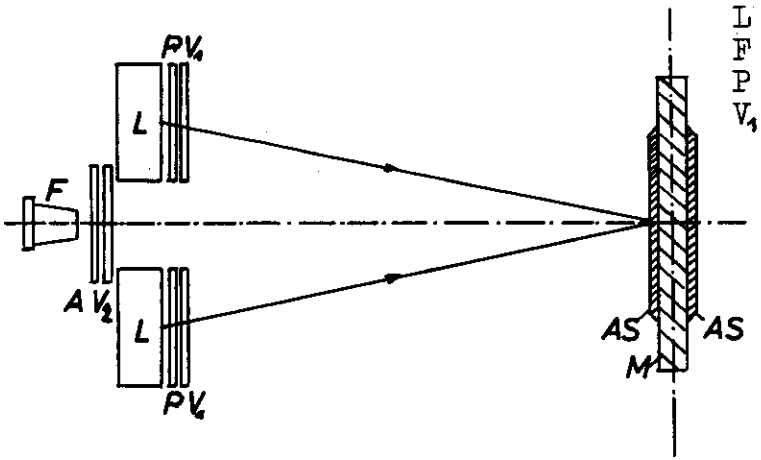

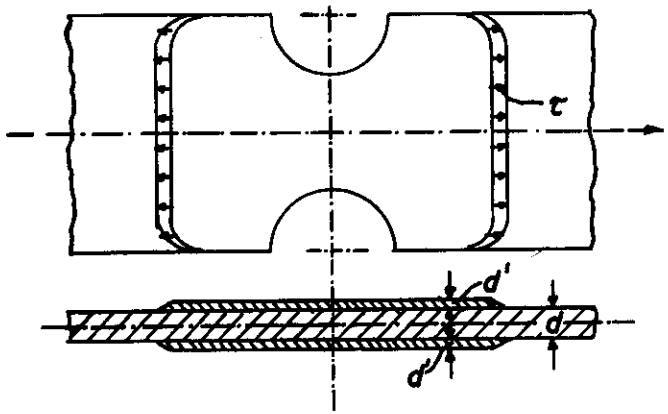

Fig.24B: Specimen with cemented Araldite layers

Fig.24A: Testing equipment for the stress-coat method (schematically)

L	Lamps	AS	Araldit-layer
F	camera	M	metal specimen
P	polariser	A	analyser
V_1 V_2	$\lambda/4$ -plates		

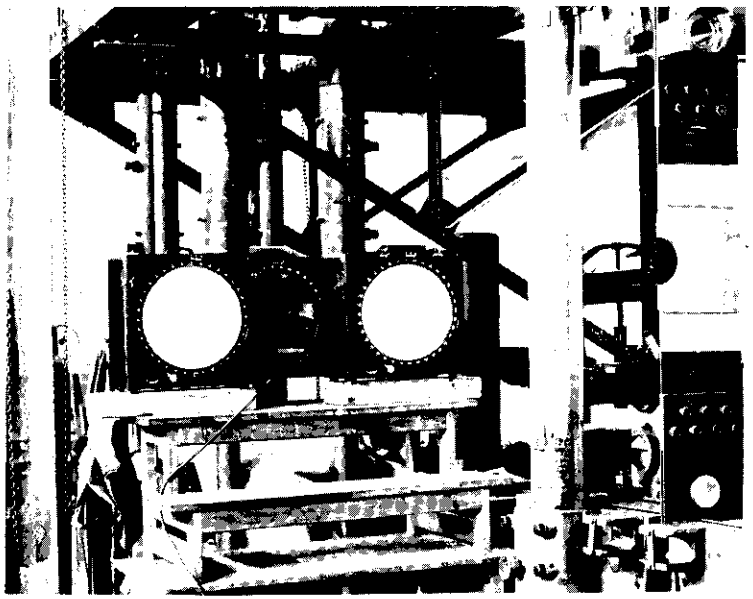

Fig.24C: Testing equipment for the stress-coat method

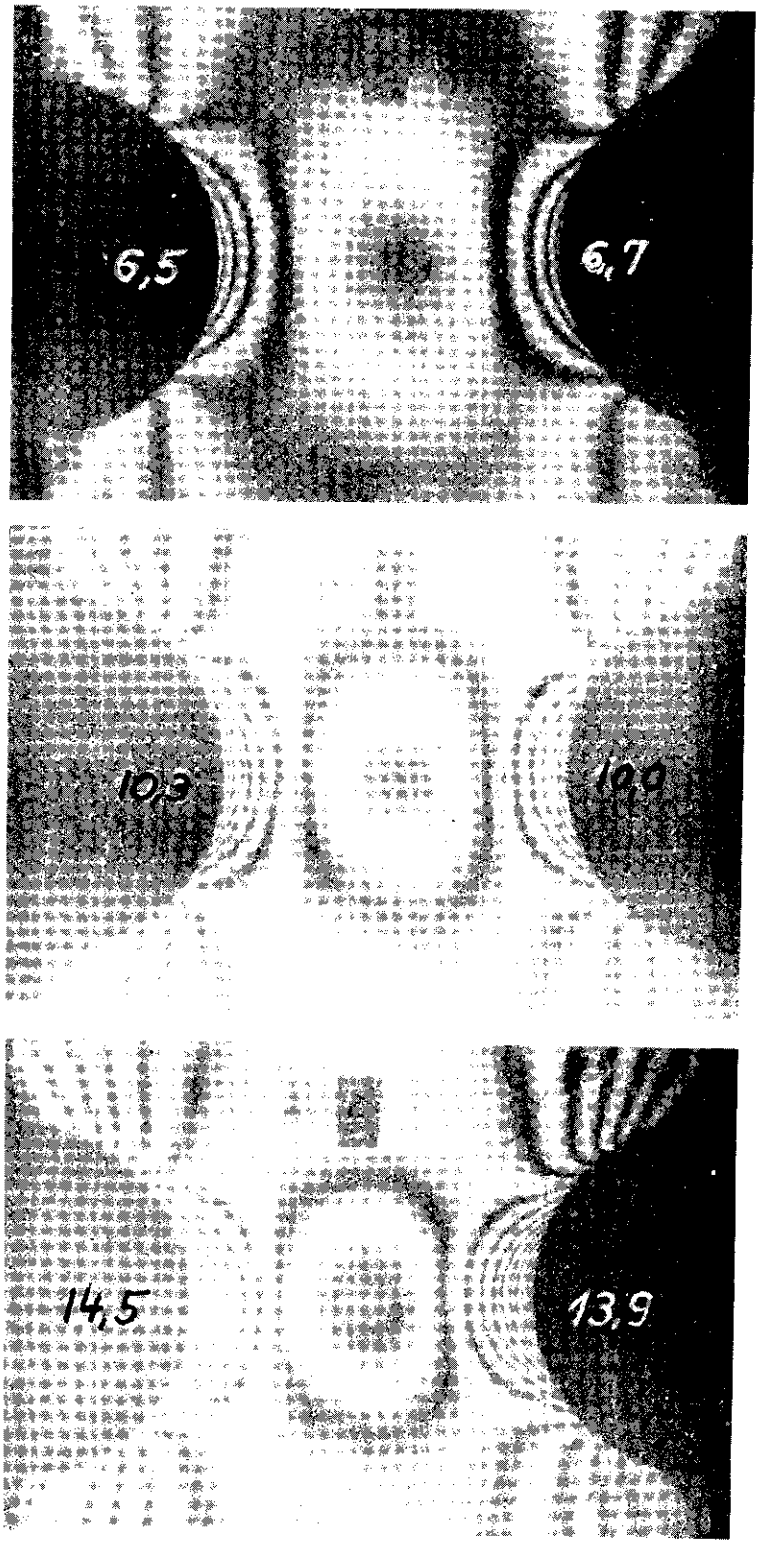

σ_N = 23,7 kg/mm^2

σ_N = 35,6 kg/mm^2

σ_N = 43,5 kg/mm^2

Fig.25: Isochromatic patterns by means of the stress-coat method for various nominal stresses σ_N (material "Velodur")

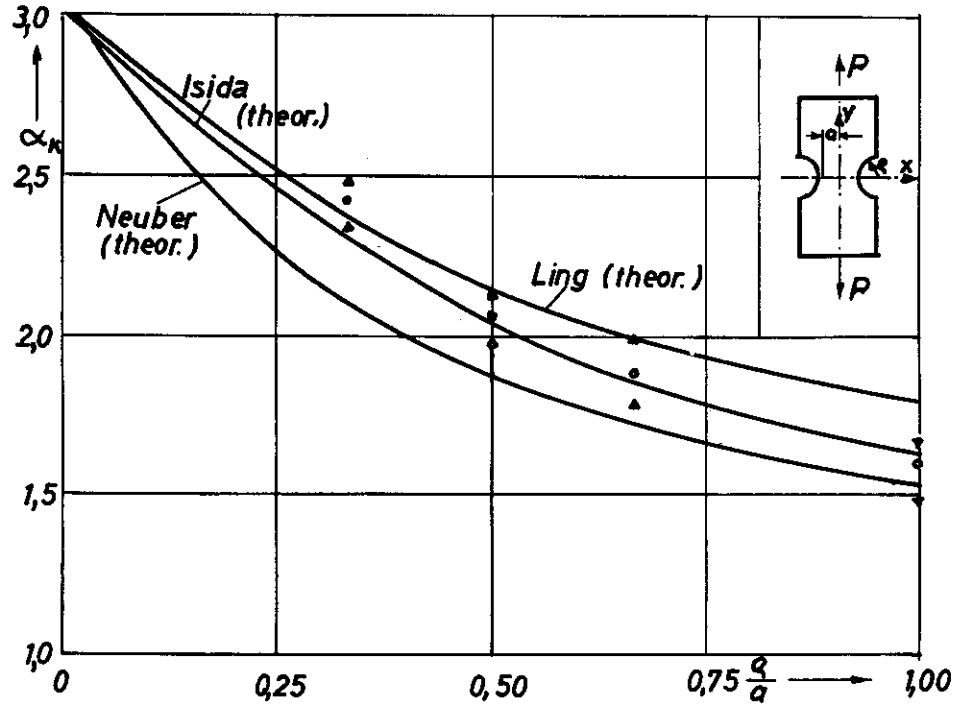

Fig.26: ESCF α vs. ρ/a for a tension strip with external notches (Δ extremal values, $\circ$ average values of the tests)

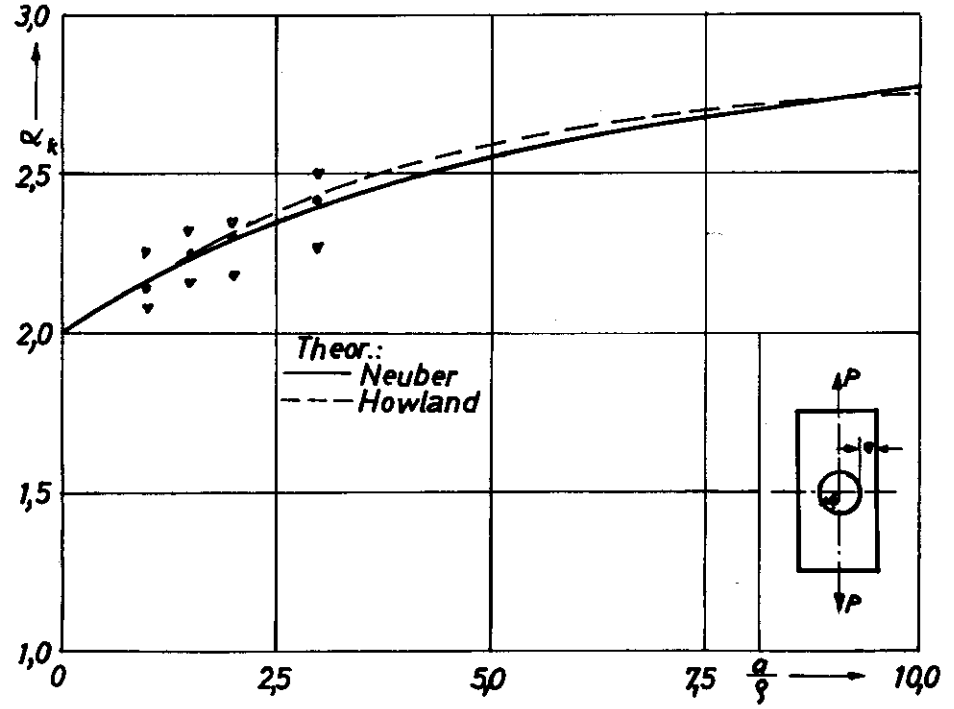

Fig.27: ESCF α vs. a/ρ for a tension strip with a central hole (∇ extremal values, $\circ$ average values of the tests)

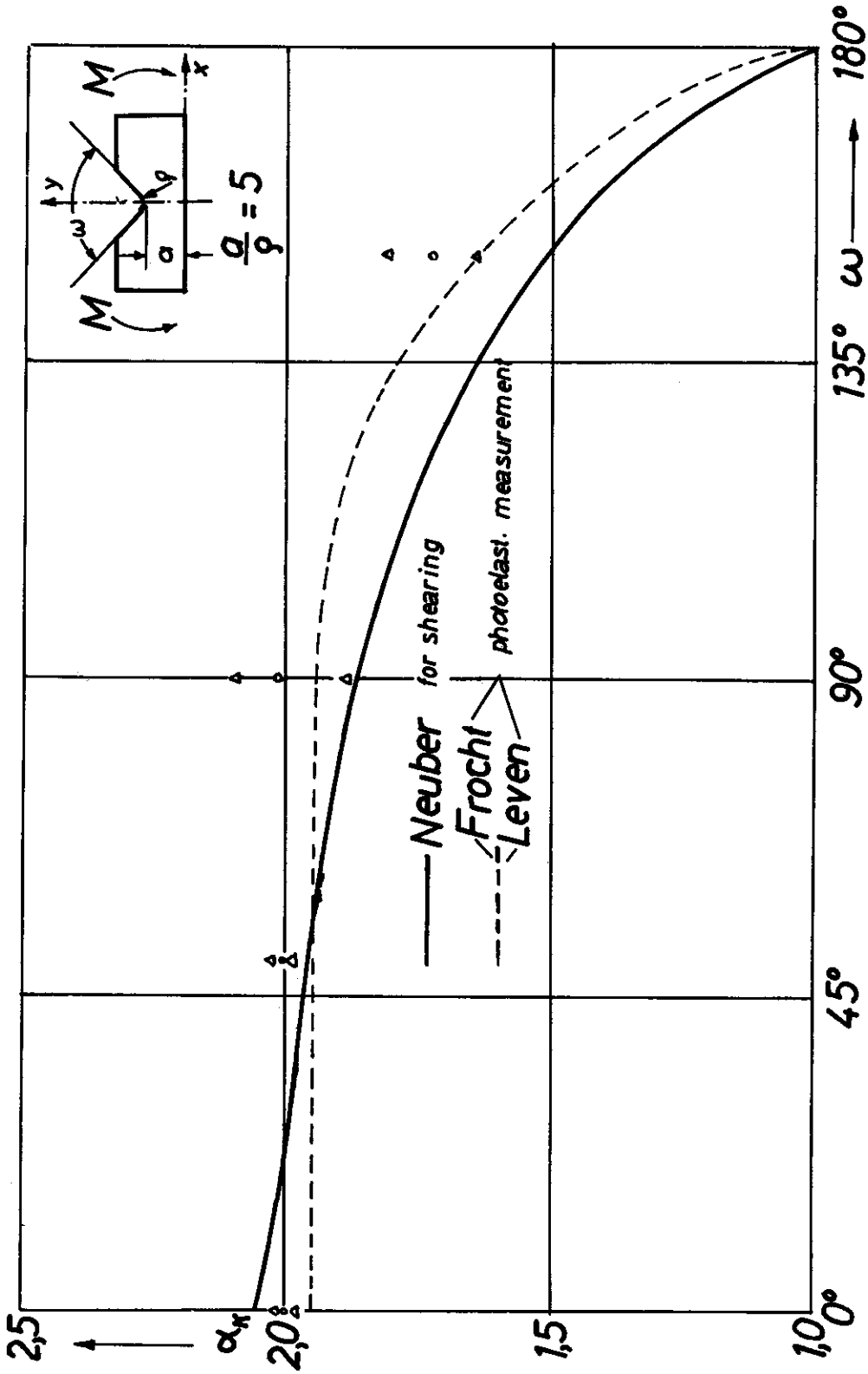

Fig.28: ESCF α vs. notch-angle ω for a single-notched bending bar (Experimental: Δ extremal values, o average values)

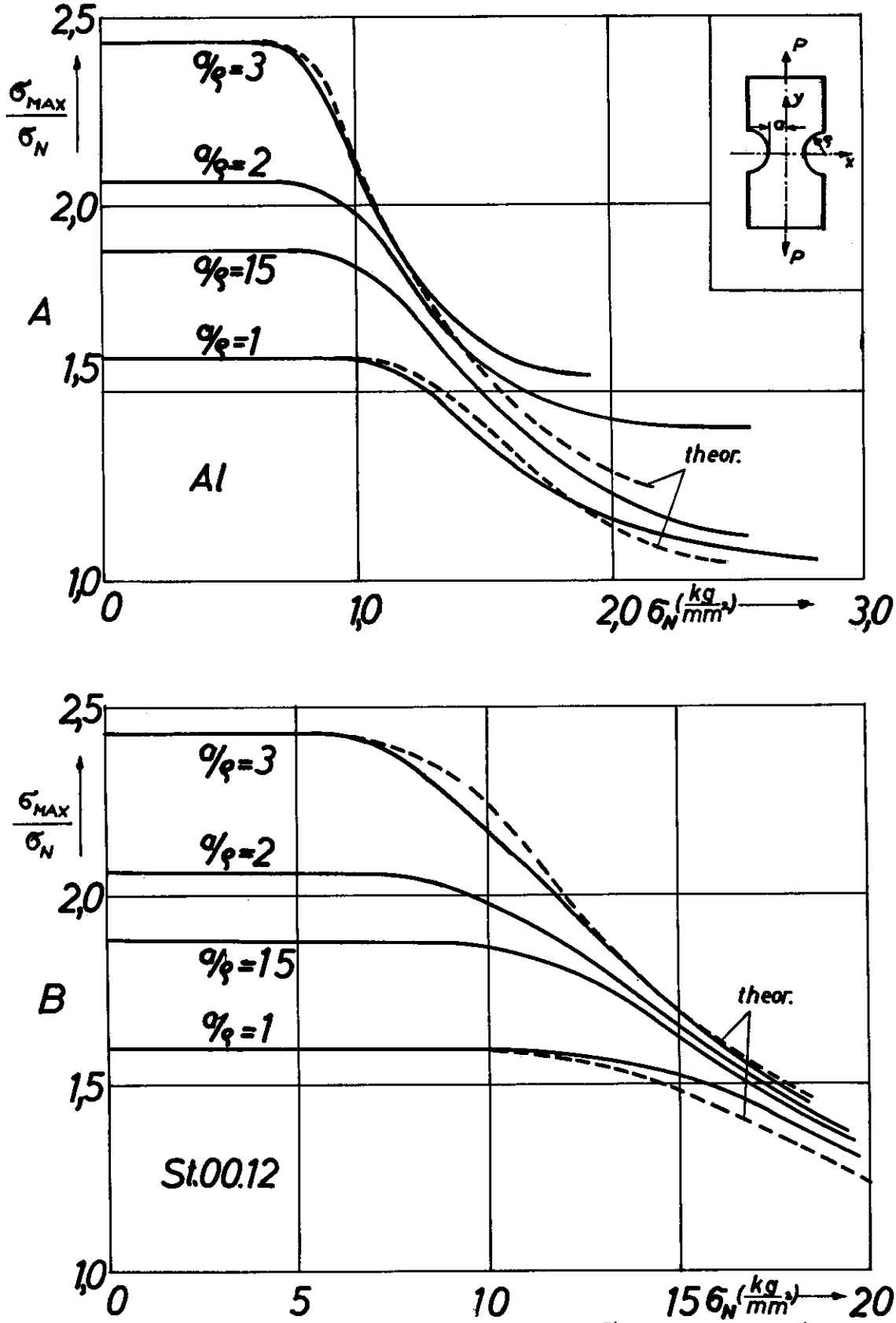

Fig.29: Experimentally determined SCF σ_{MAX}/σ_N vs. σ_N for a tension strip with external notches and various ratios a/ρ (materials: Aluminum and steel St.00.12)

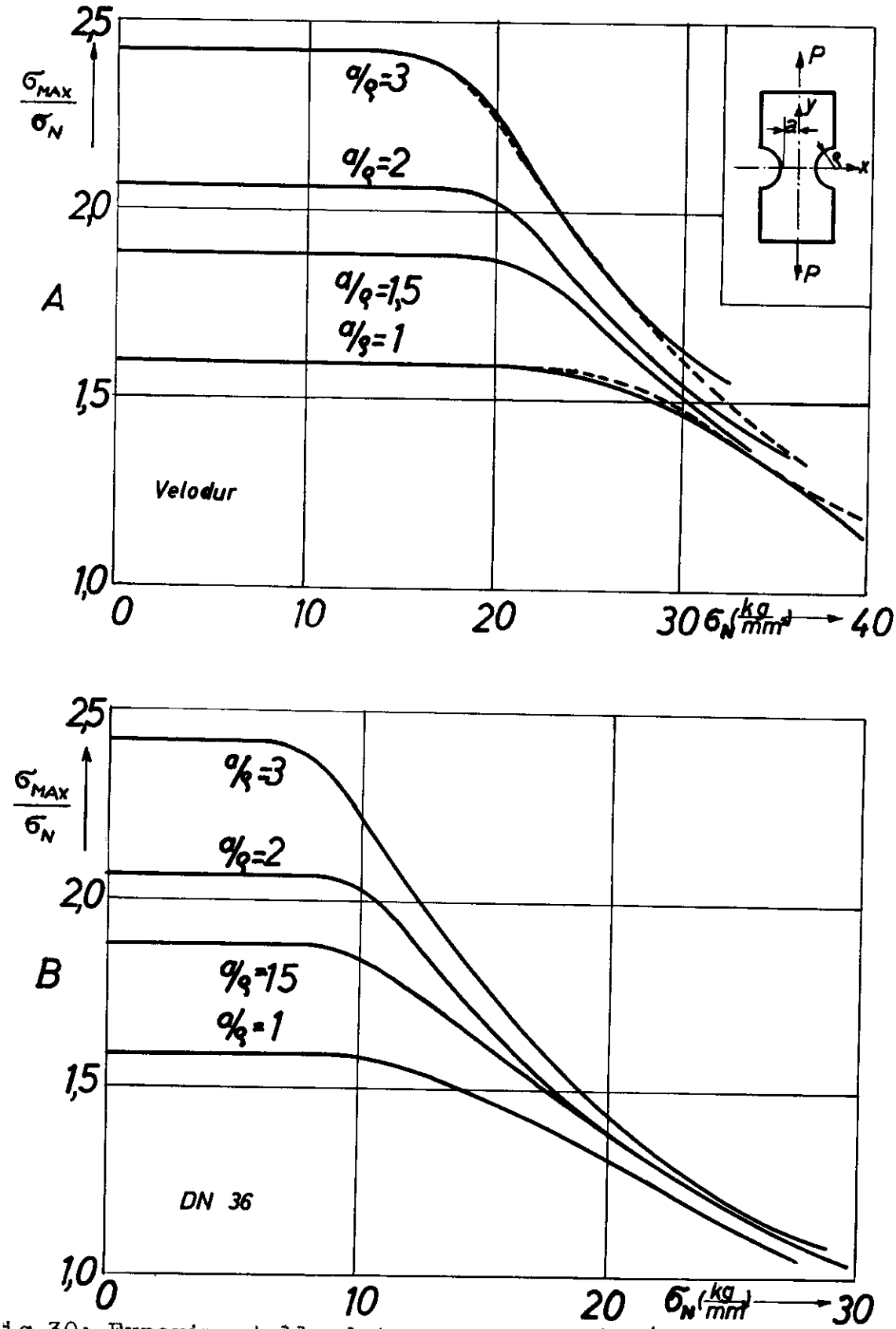

Fig.30: Experimentally determined SCF σ_{MAX}/σ_N vs. for a tension strip with external notches and various ratios a/ρ (materials: Velodur and special steel DN 36)

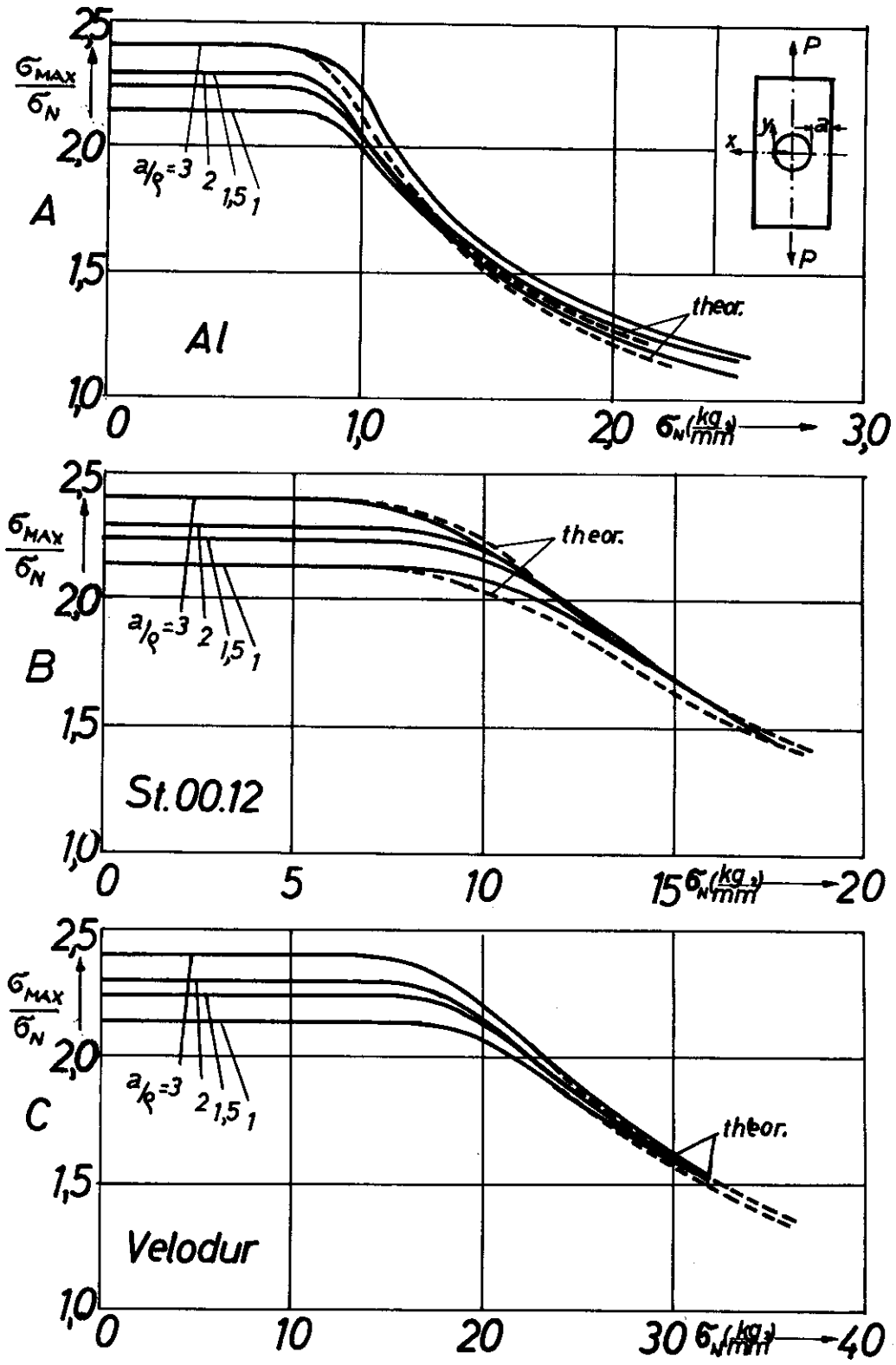

Fig.31: Experimentally determined SCF σ_{MAX}/σ_N vs. σ_N for a tension strip with a central hole and various ratios a/ρ (materials: Aluminum, St.00.12, Velodur)

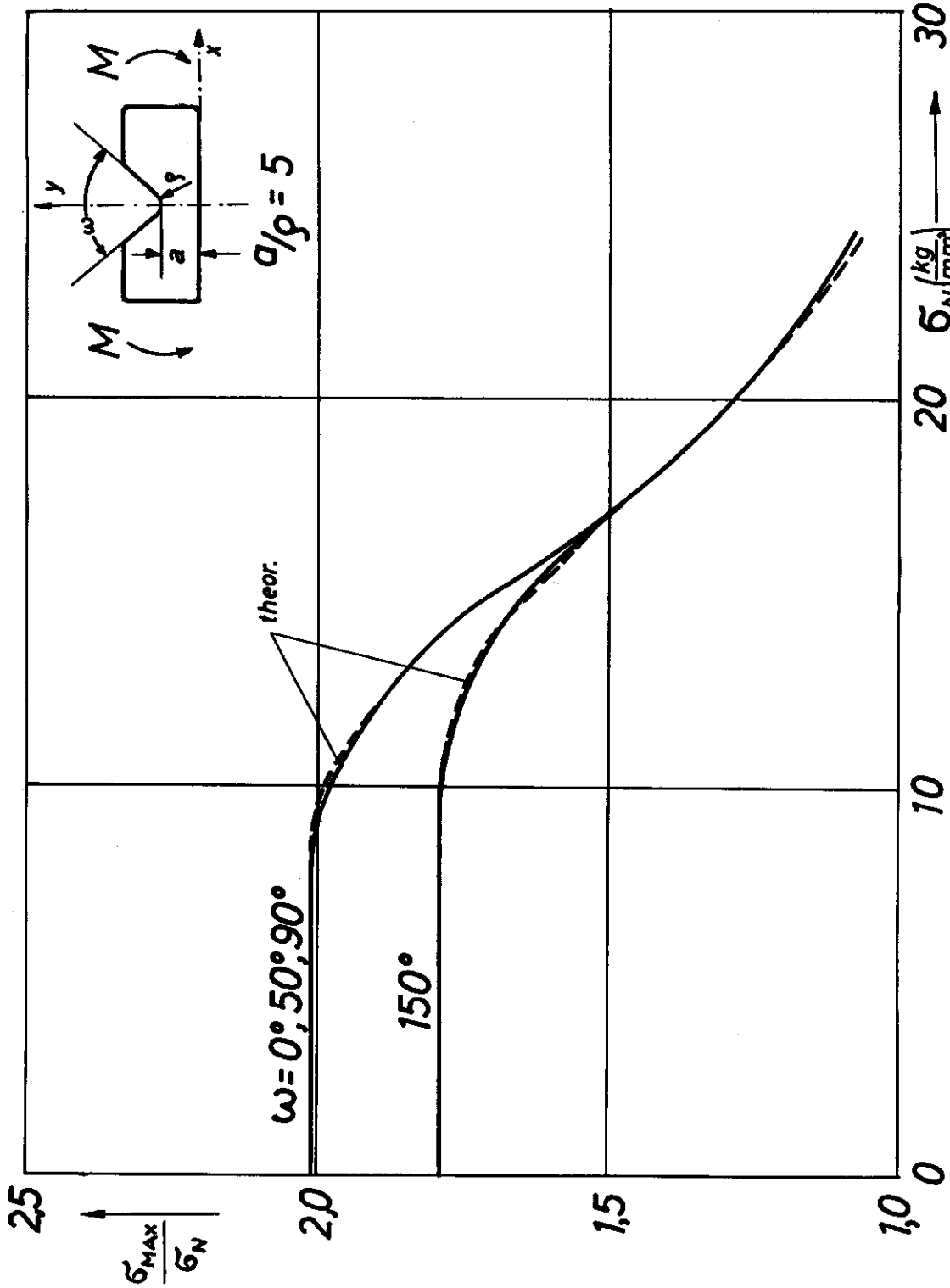

Fig.32: Experimentally determined SCF σ_{MAX}/σ_N vs. σ_N for a single-notched bending bar and various notch-angles ω (material: Steel St.00.21)

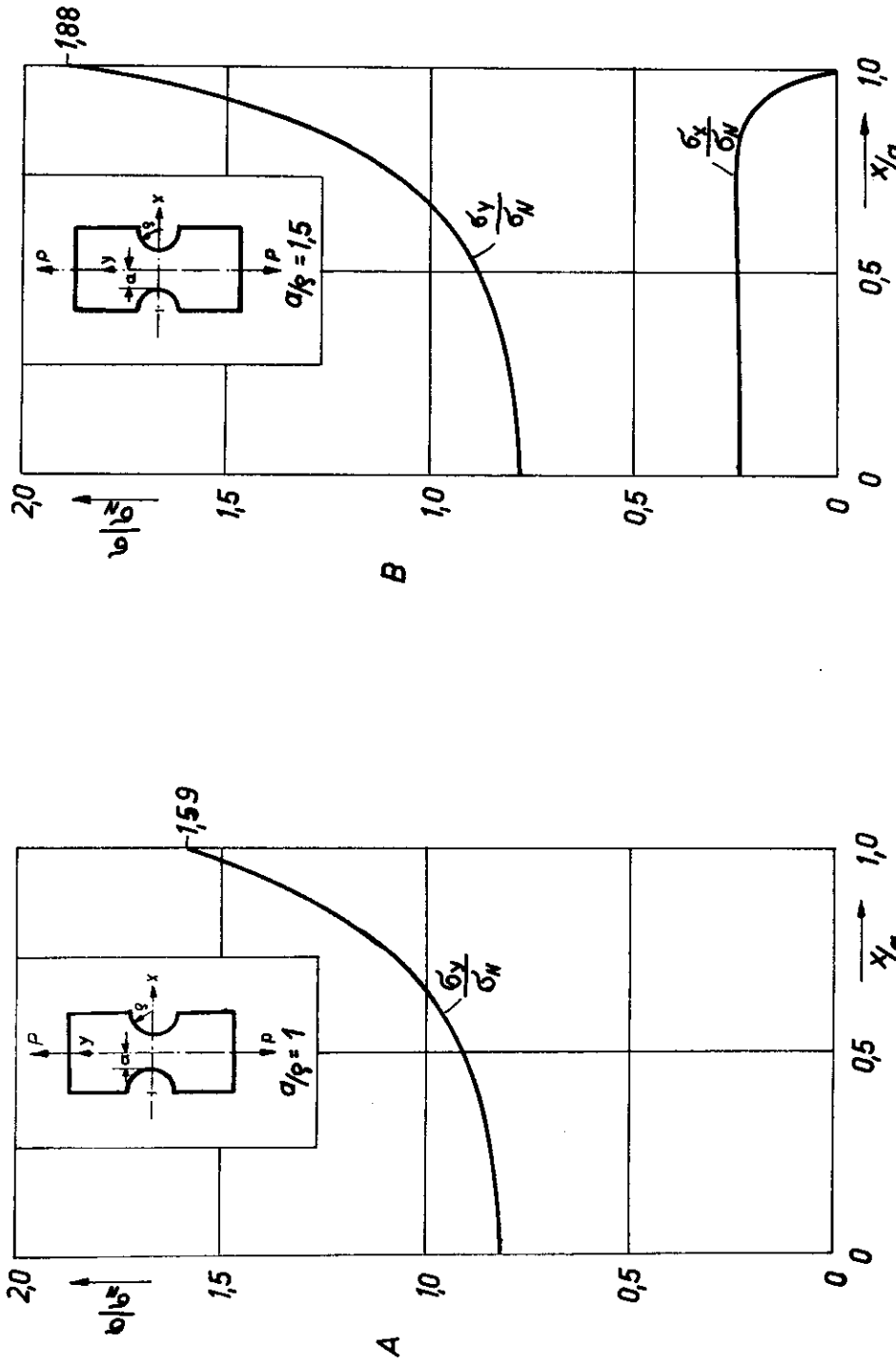

Fig.33: Experimentally determined stress distribution over the minimum section of a tension strip with external notches for $a/\rho = 1,0$ and $a/\rho = 1,5$ (elastic range)

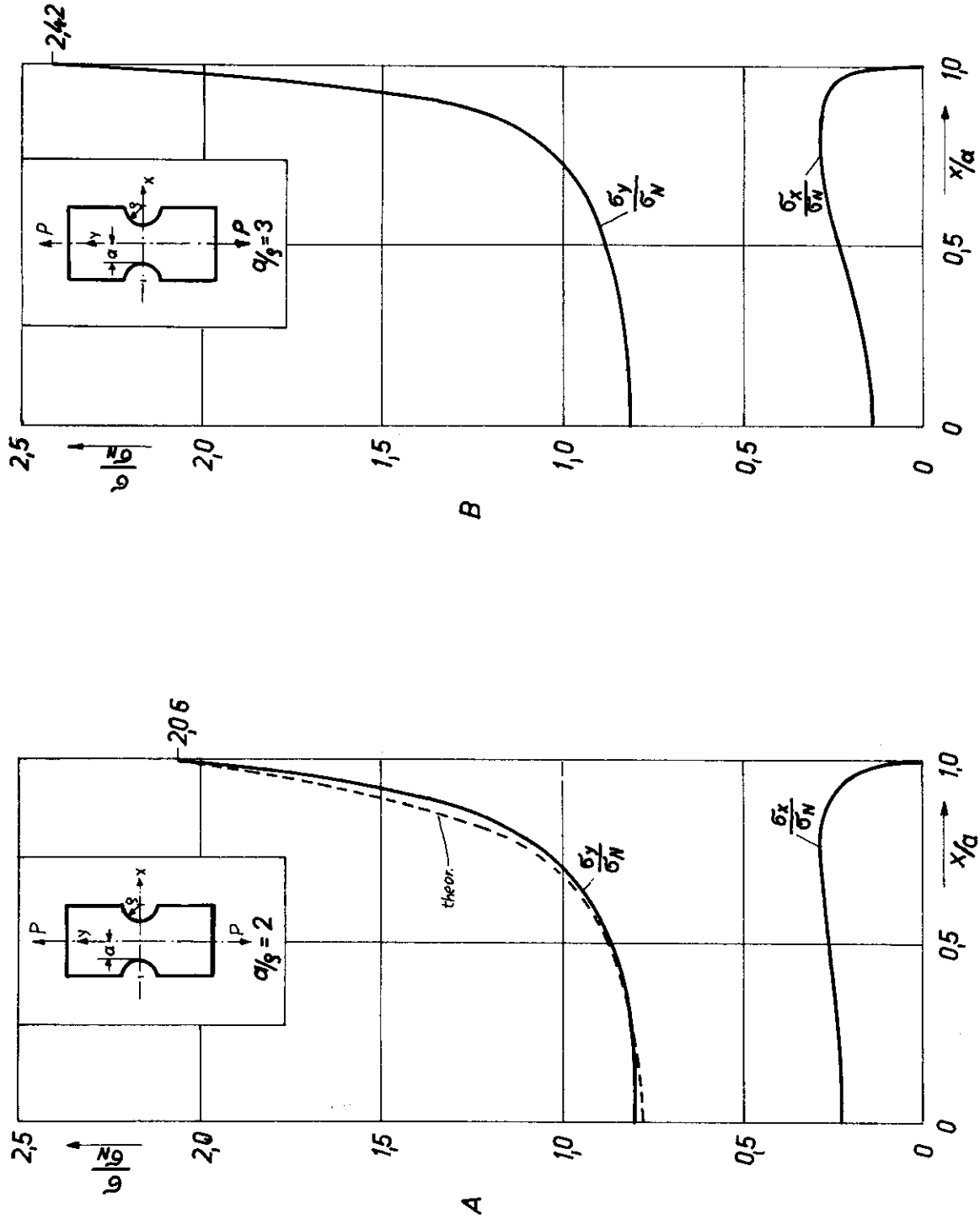

Fig.34: Experimentally determined stress distribution over the minimum section of a tension strip with external notches for $a/\rho = 2,0$ and $a/\rho = 3,0$ (elastic range)

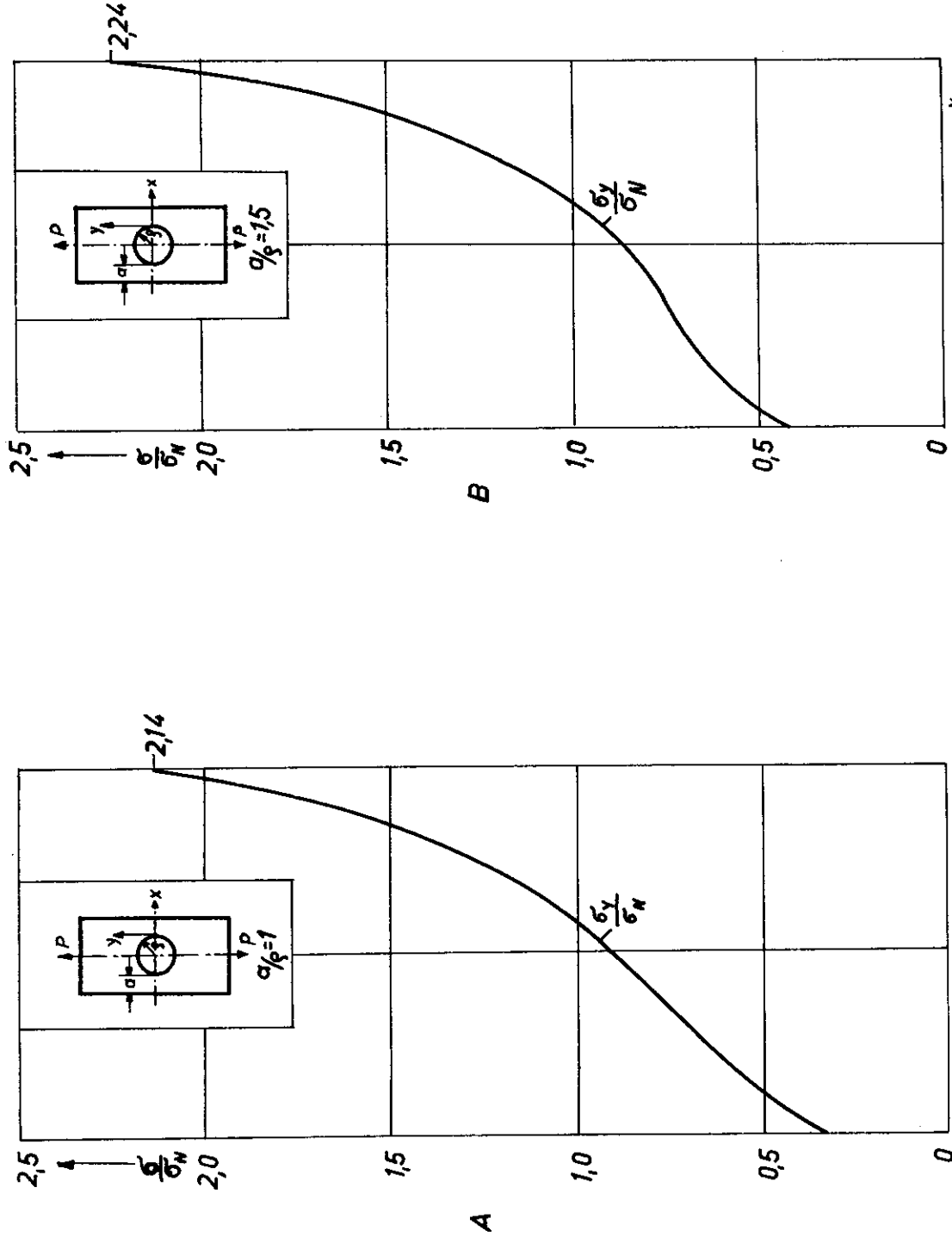

Fig.35: Experimentally determined stress distribution over the minimum section of a tension strip with a central hole for $a/\rho = 1,0$ and $a/\rho = 1,5$ (elastic range)

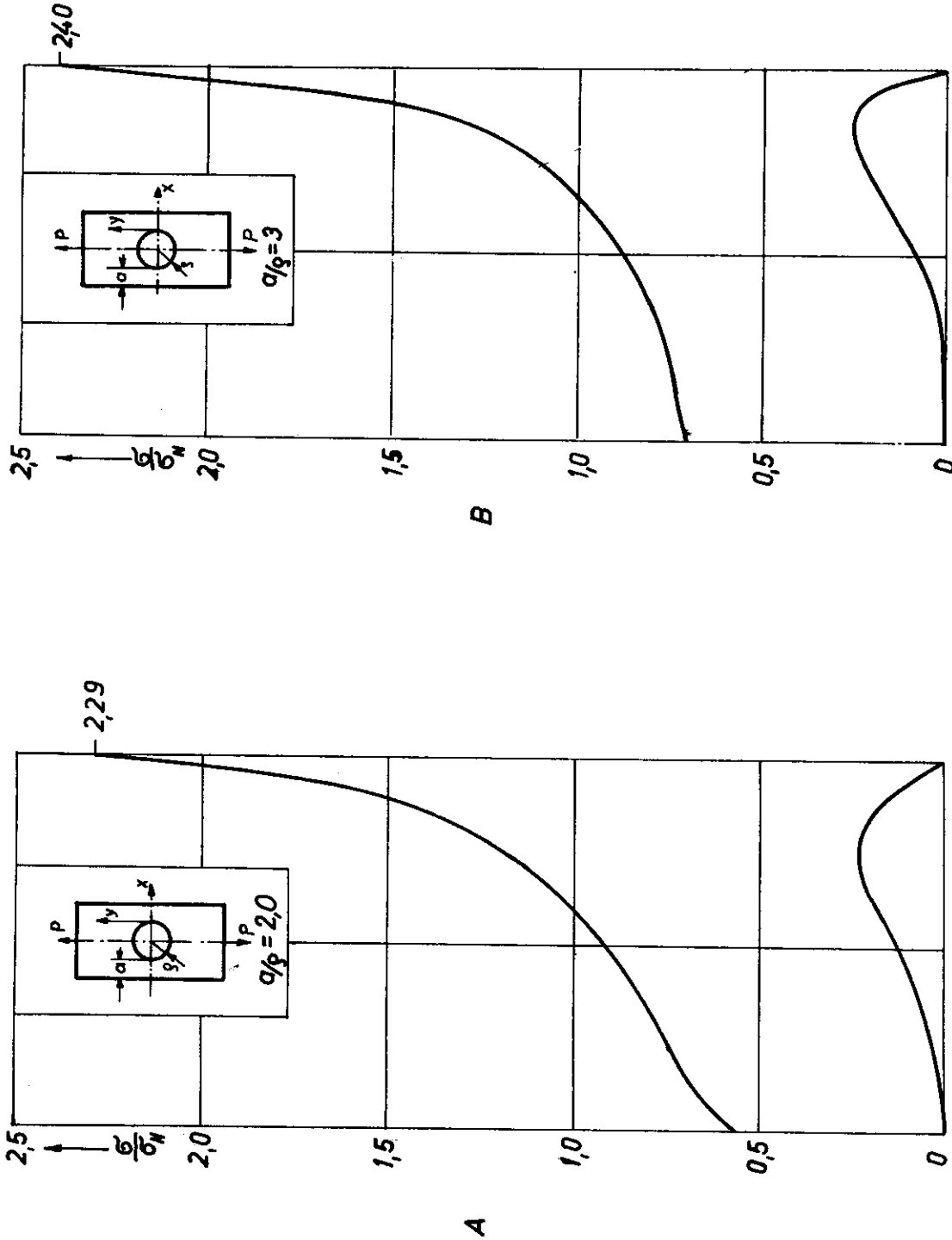

Fig. 36: Experimentally determined stress distribution over the minimum section of a tension strip with a central hole for $a/\rho = 2,0$ and $a/\rho = 3,0$ (elastic range)

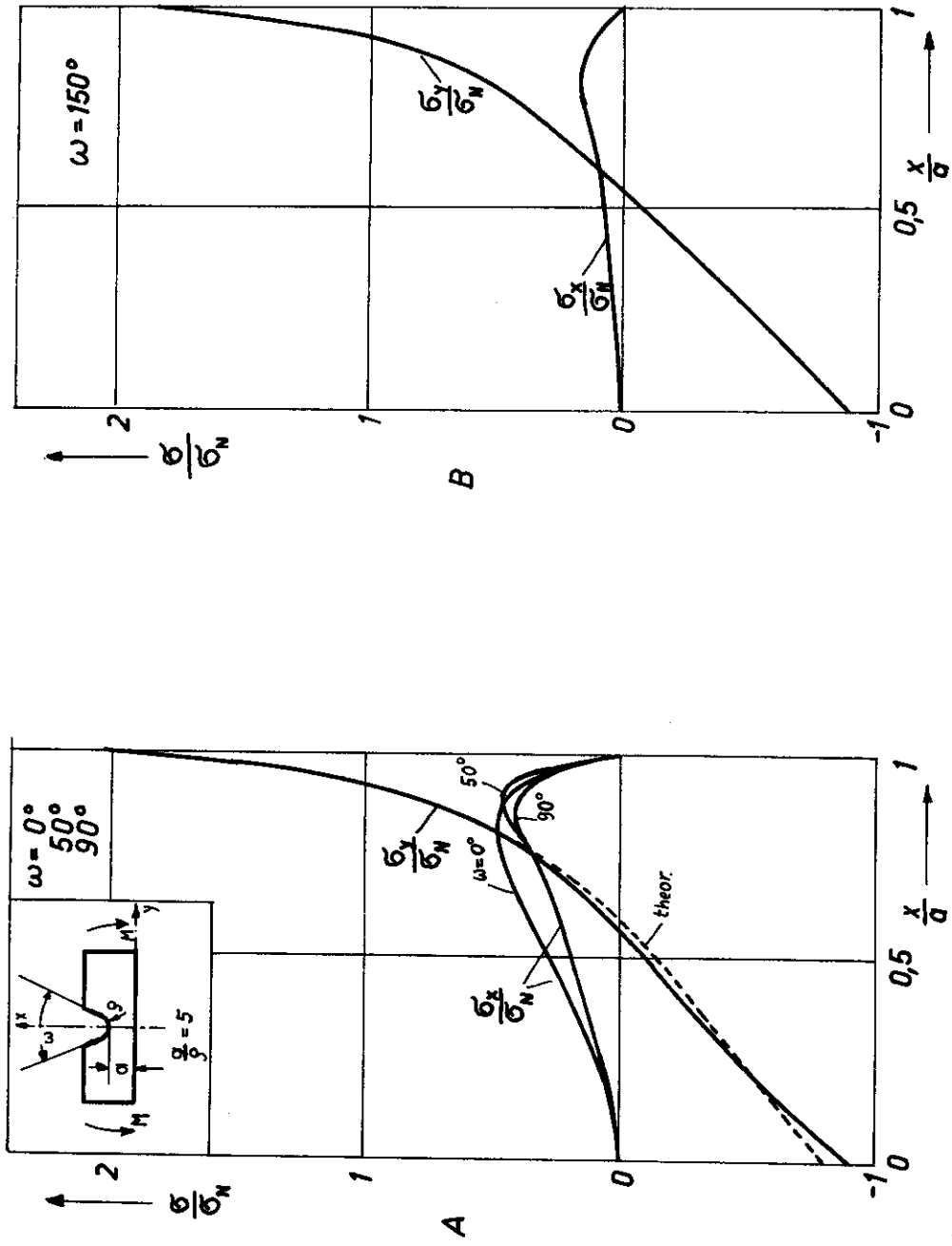

Fig.37: Experimentally determined stress distribution over the minimum section of a single-notched bending bar for ω = 0°, 50°, 90° and 1500 (elastic range)

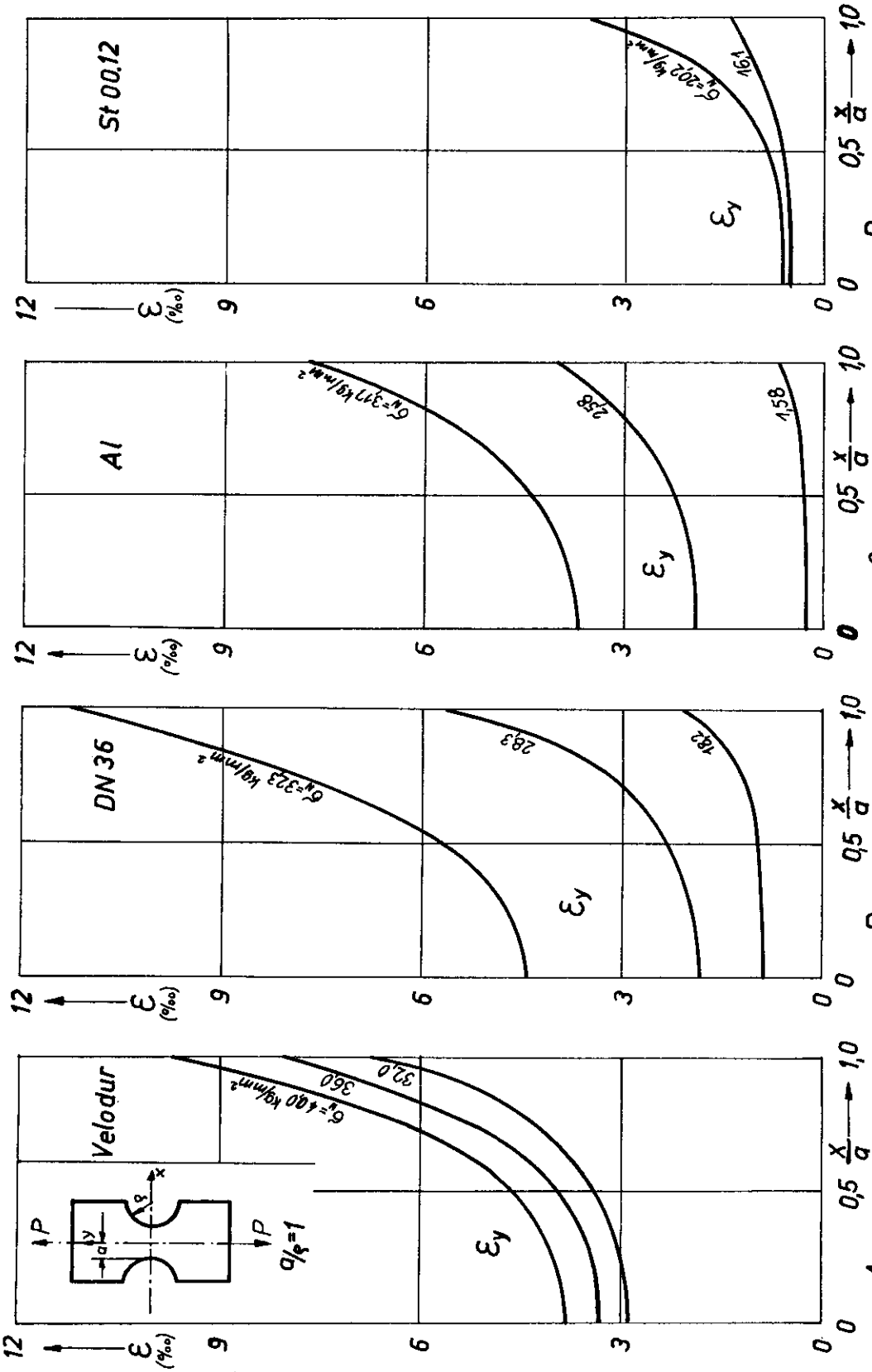

Fig.38: Experimentally determined strain distribution over the minimum section of a tension strip with external notches (a/ϱ = 1,0) for various nominal stresses (materials: Velodur, special steel DN 36, steel St.00.12, Aluminum) (plastic range)

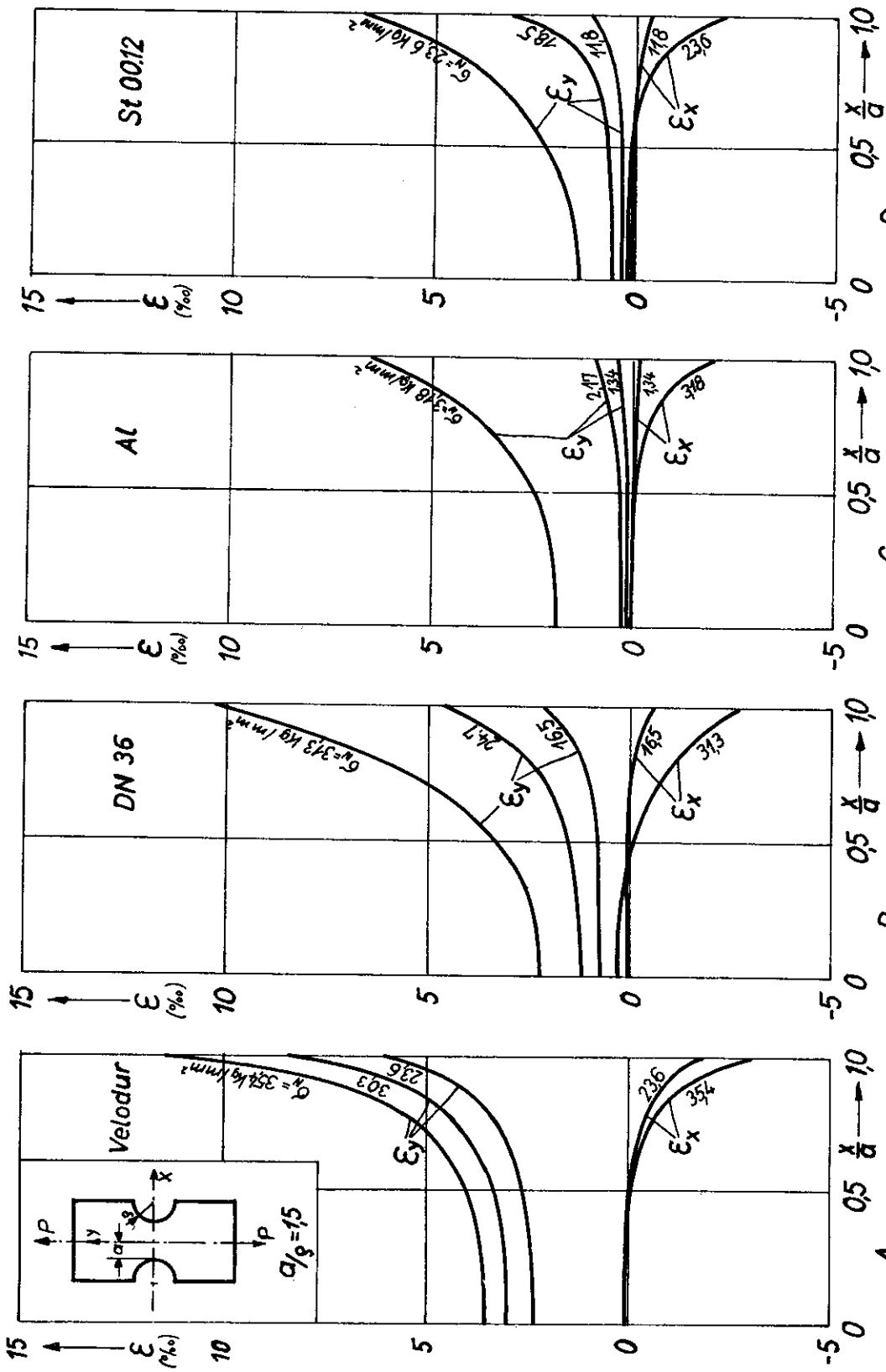

Fig.39: Experimentally determined strain distribution over the minimum section of a tension strip with external notches ($a/\rho = 1{,}5$) for various nominal stresses (materials: Velodur, special steel DN 36, steel St.00.12, Aluminum) (plastic range)

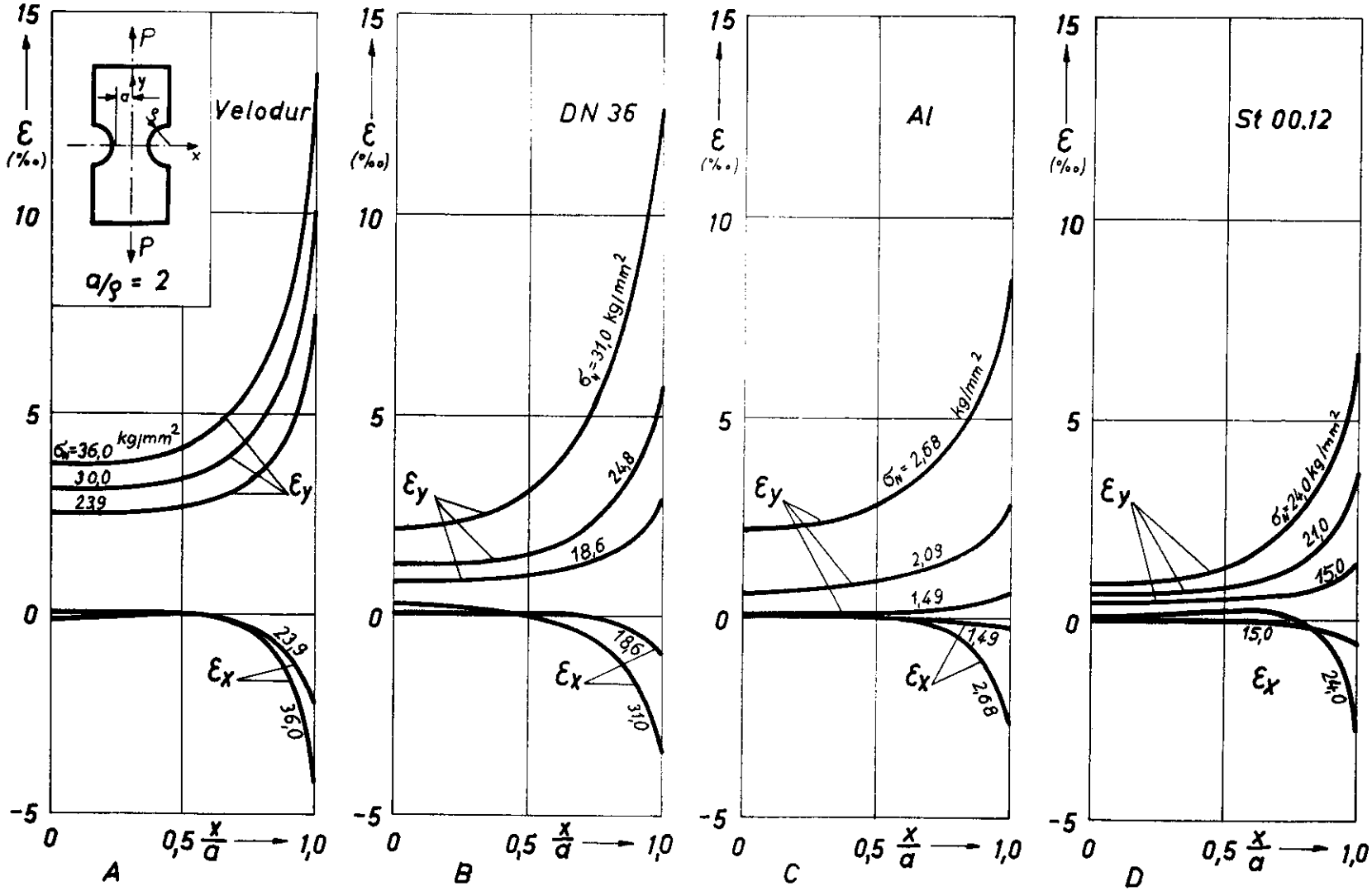

Fig.40: Experimentally determined strain distribution over the minimum section of a tension strip with external notches (a/ϱ = 2,0) for various nominal stresses (materials: Velodur, special steel DN 36, steel St.00.12, Aluminum)(plastic range)

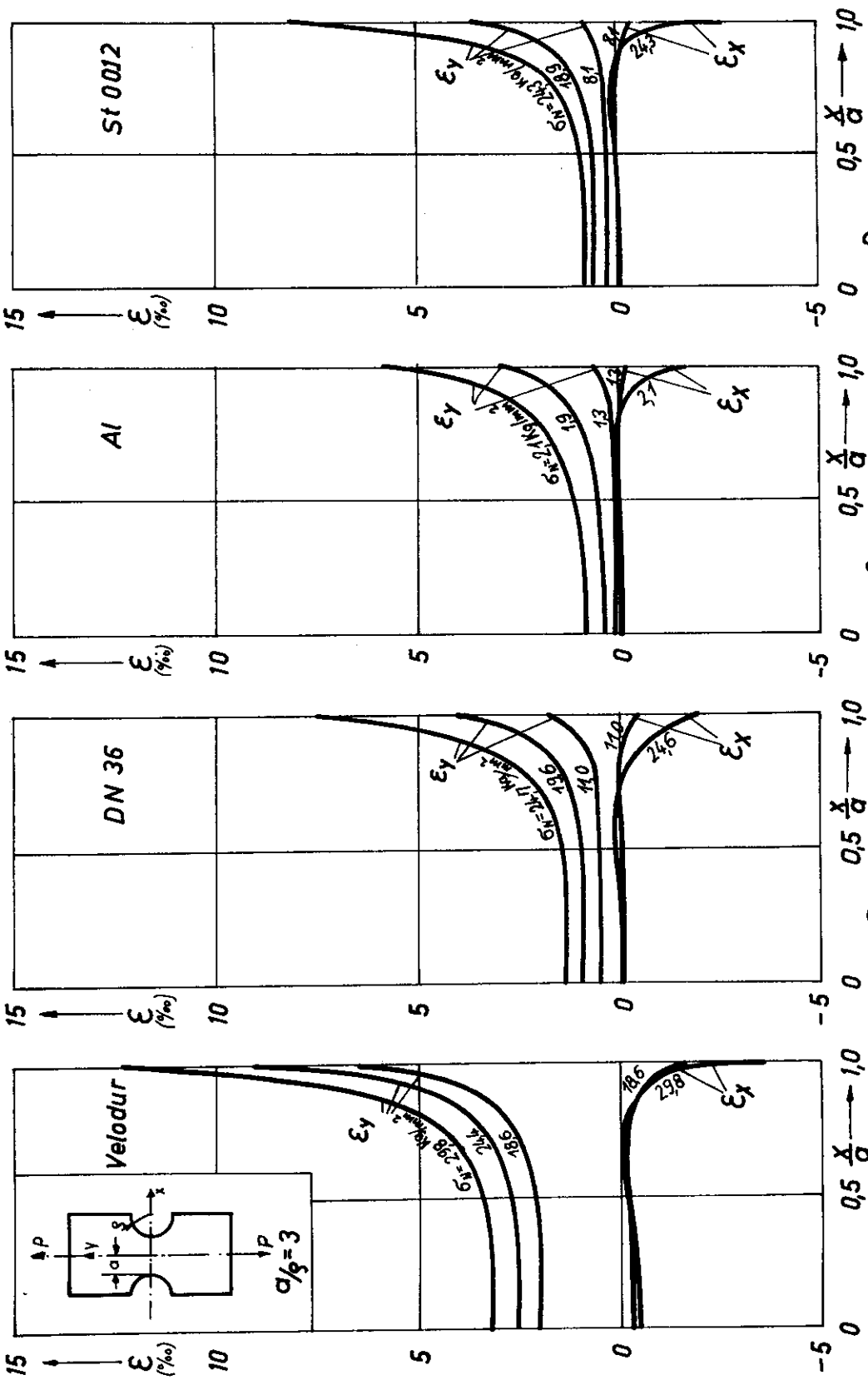

Fig.41: Experimentally determined strain distribution over the minimum section of a tension strip with external notches ($\alpha/\rho = 3{,}0$) for various nominal stresses (materials: Velodur, special steel DN 36, steel St.00.12, Aluminum) (plastic range)

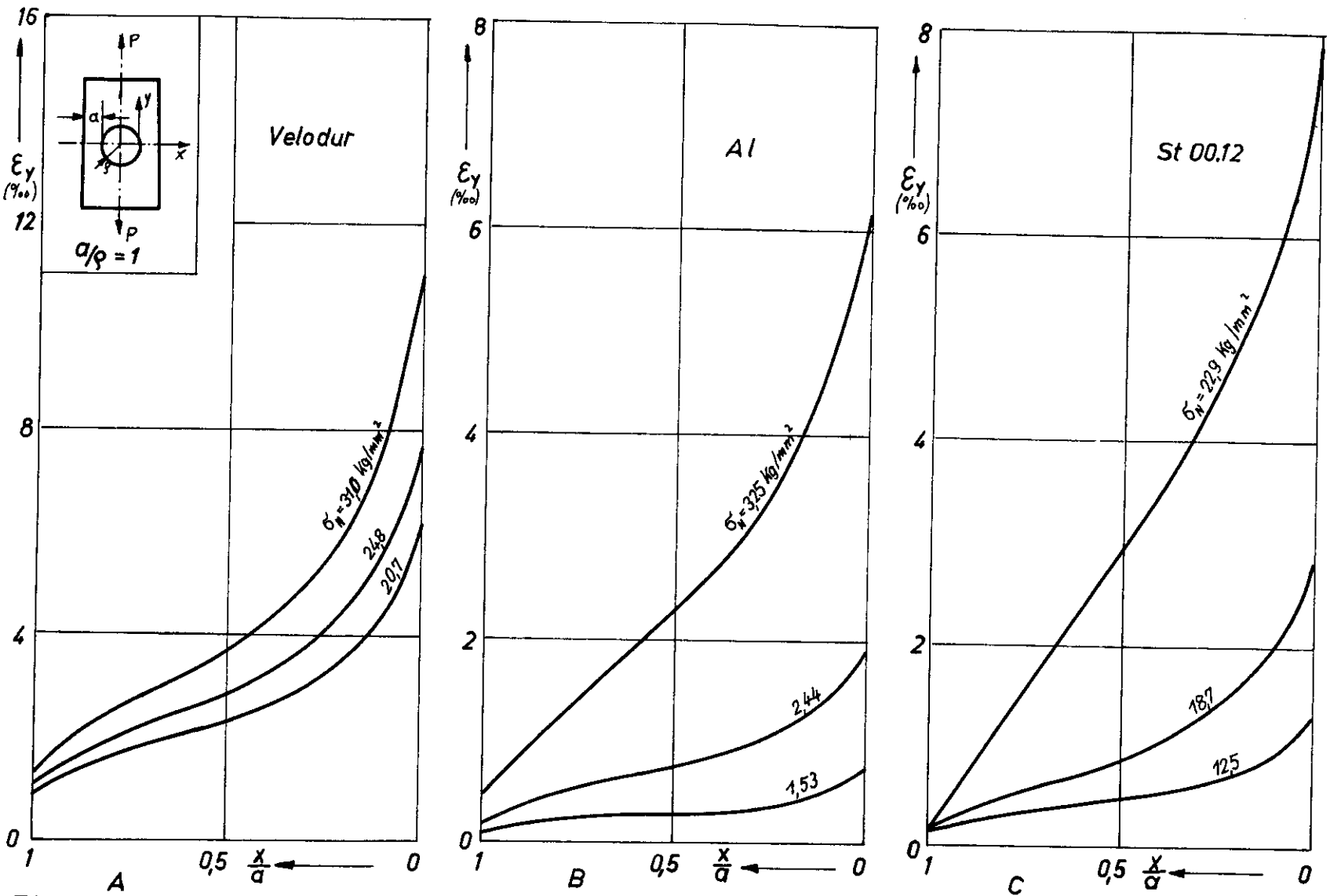

Fig.42: Experimentally determined strain distribution over the minimum section of a tension strip with a central hole ($a/\rho = 1{,}0$) for various nominal stresses (materials: Velodur, steel St.00.12, Aluminum) (plastic range)

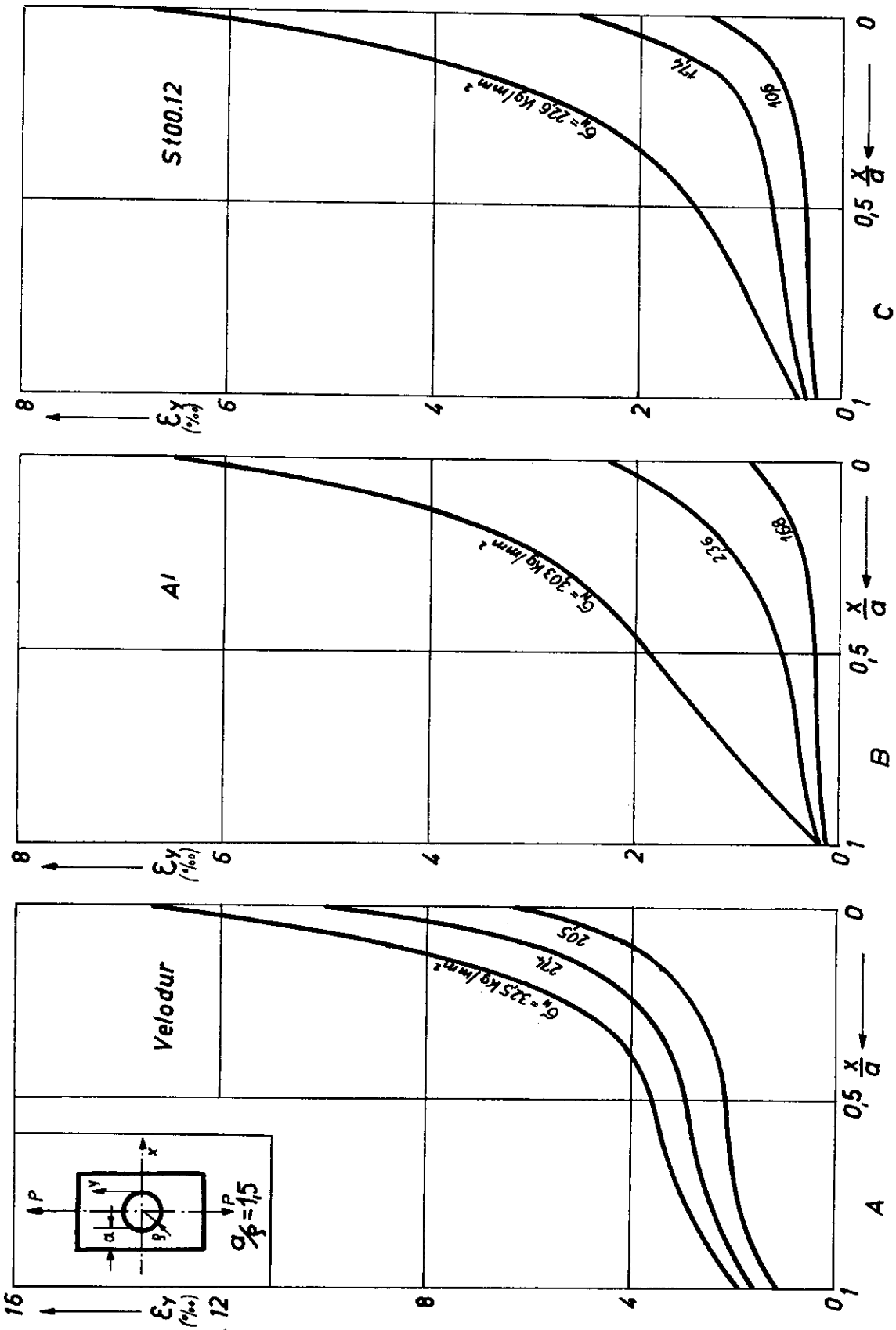

Fig.43: Experimentally determined strain distribution over the minimum section of a tension strip with a central hole ($a/b = 1,5$) for various nominal stresses (materials: Velodur, steel St.00.12, Aluminum) (plastic range)

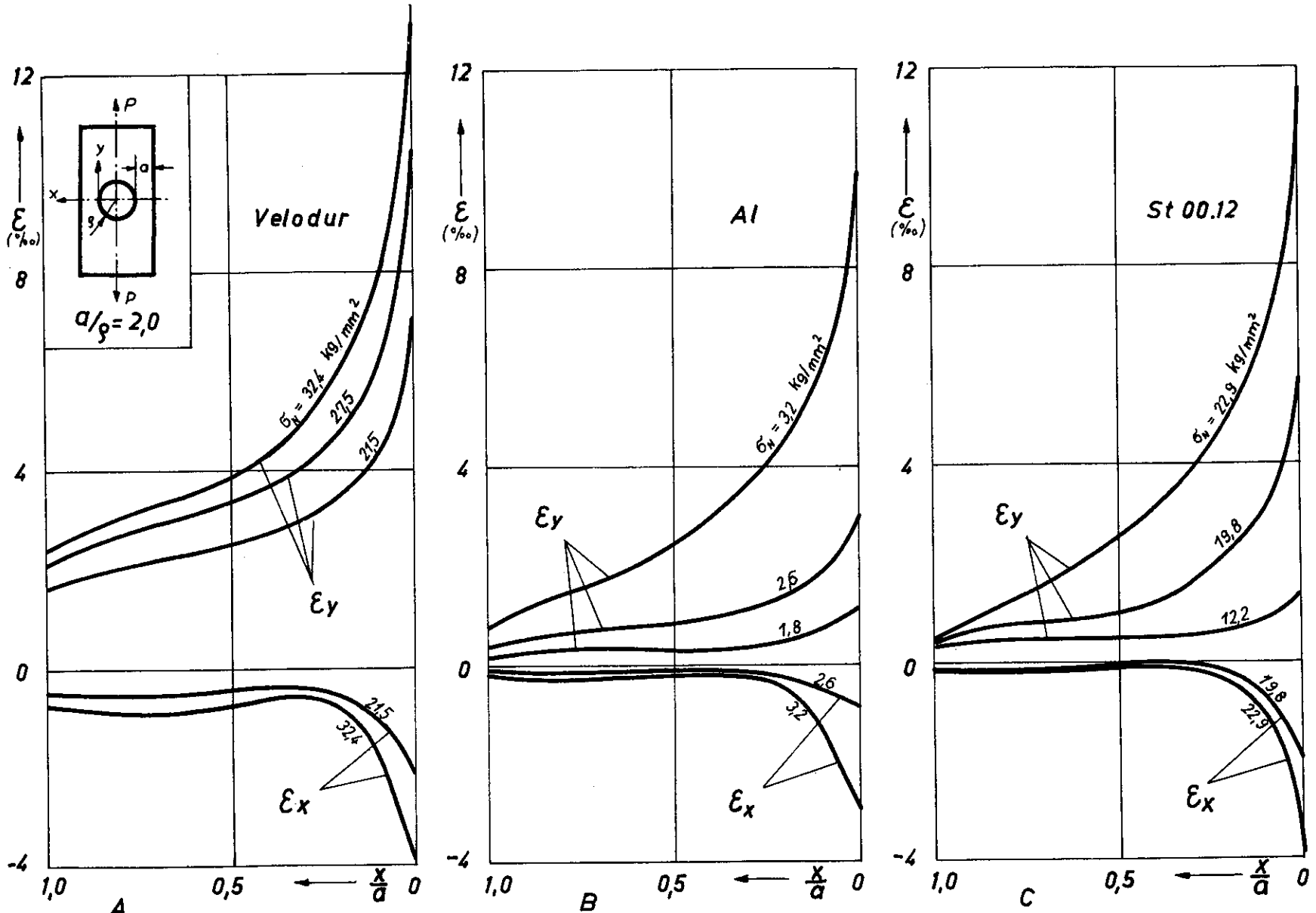

Fig.44: Experimentally determined strain distribution over the minimum section of a tension strip with a central hole ($a/\rho = 2,0$) for various nominal stresses (materials: Velodur, steel St.00.12, Aluminum) (plastic range)

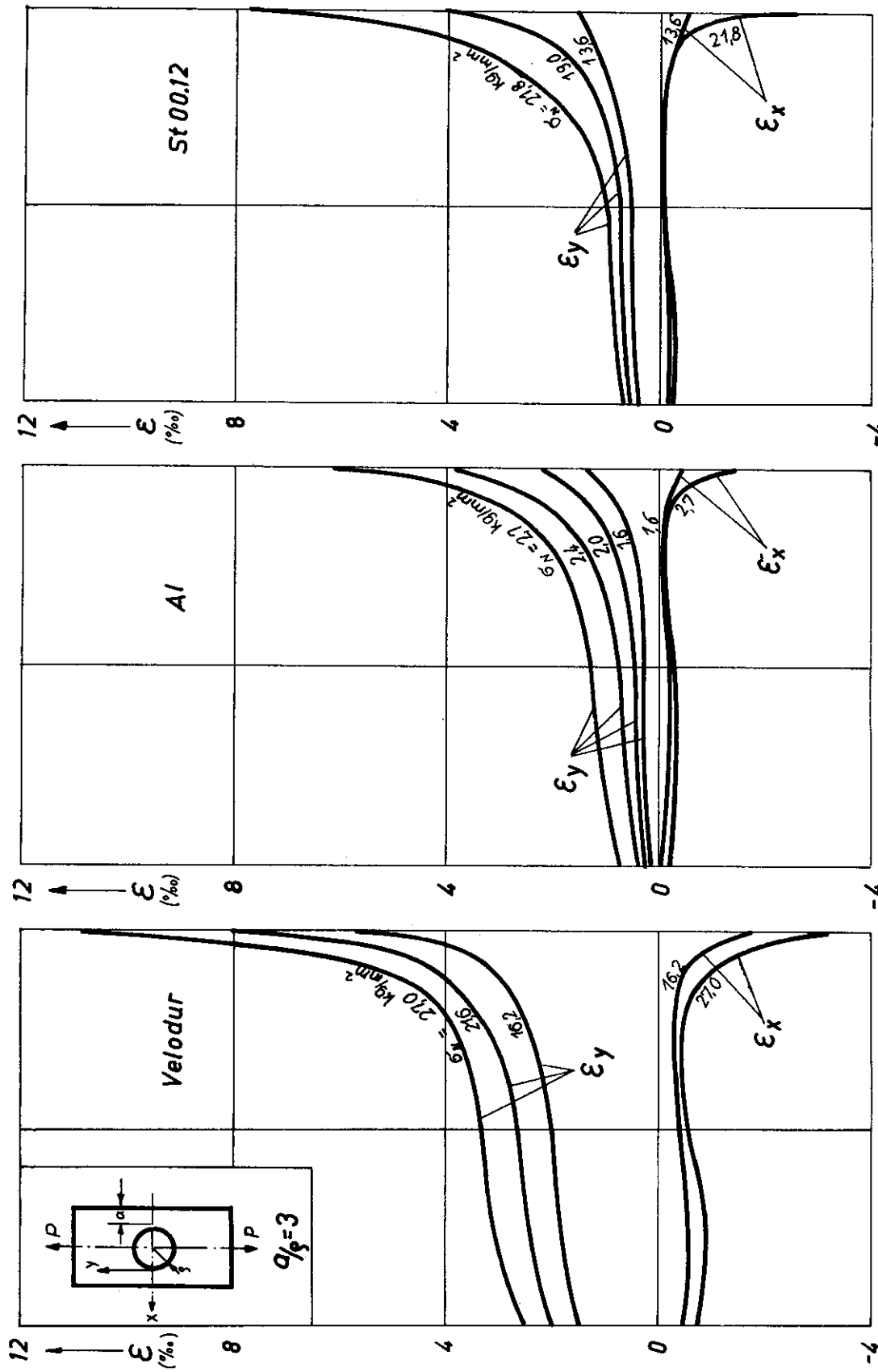

Fig.45: Experimentally determined strain distribution over the minimum section of a tension strip with a central hole ($a/\rho = 3{,}0$) for various nominal stresses (materials: Velodur, steel St.00.12, Aluminum) (plastic range)

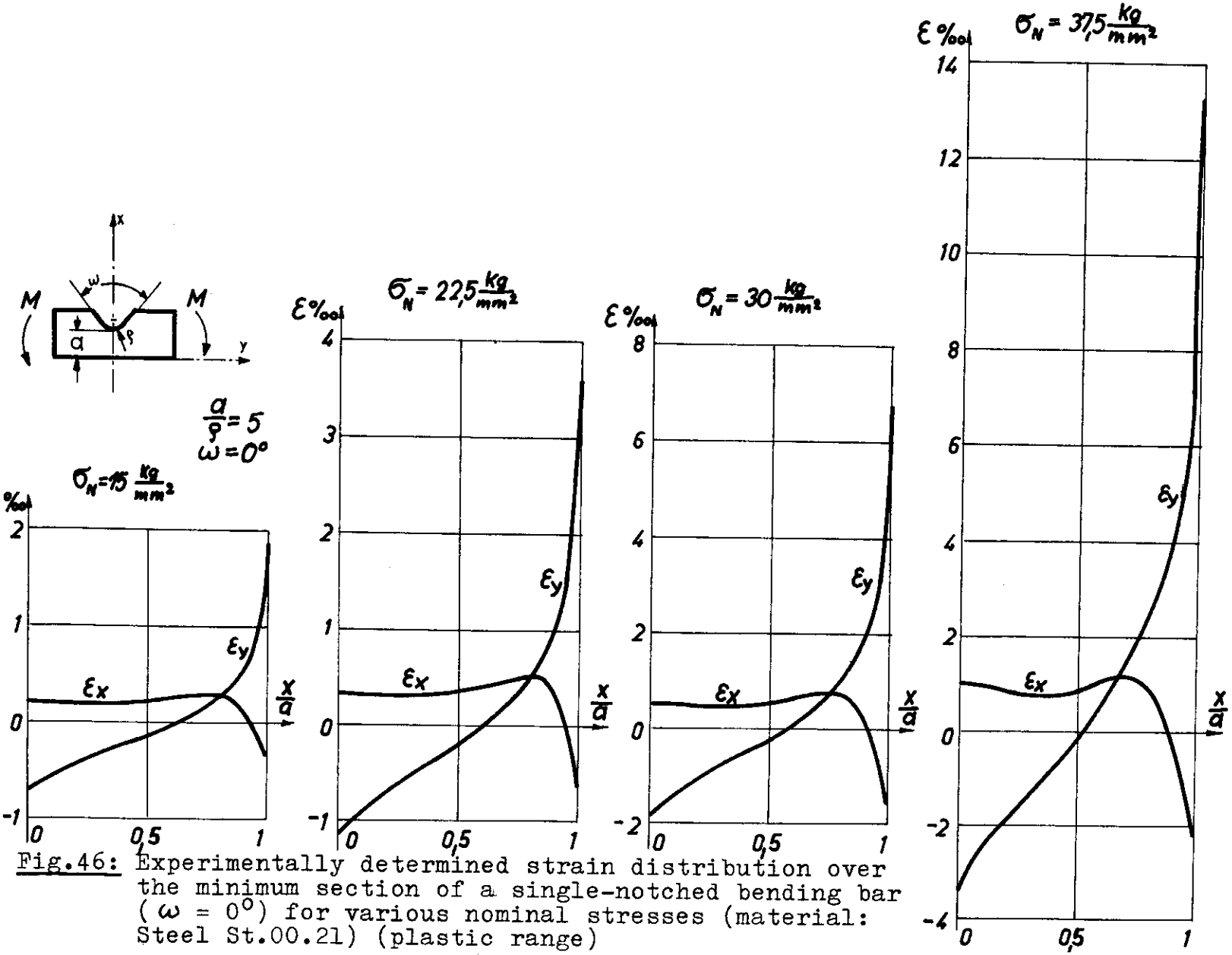

Fig.46: Experimentally determined strain distribution over the minimum section of a single-notched bending bar ($\omega = 0^{\circ}$) for various nominal stresses (material: Steel St.00.21) (plastic range)

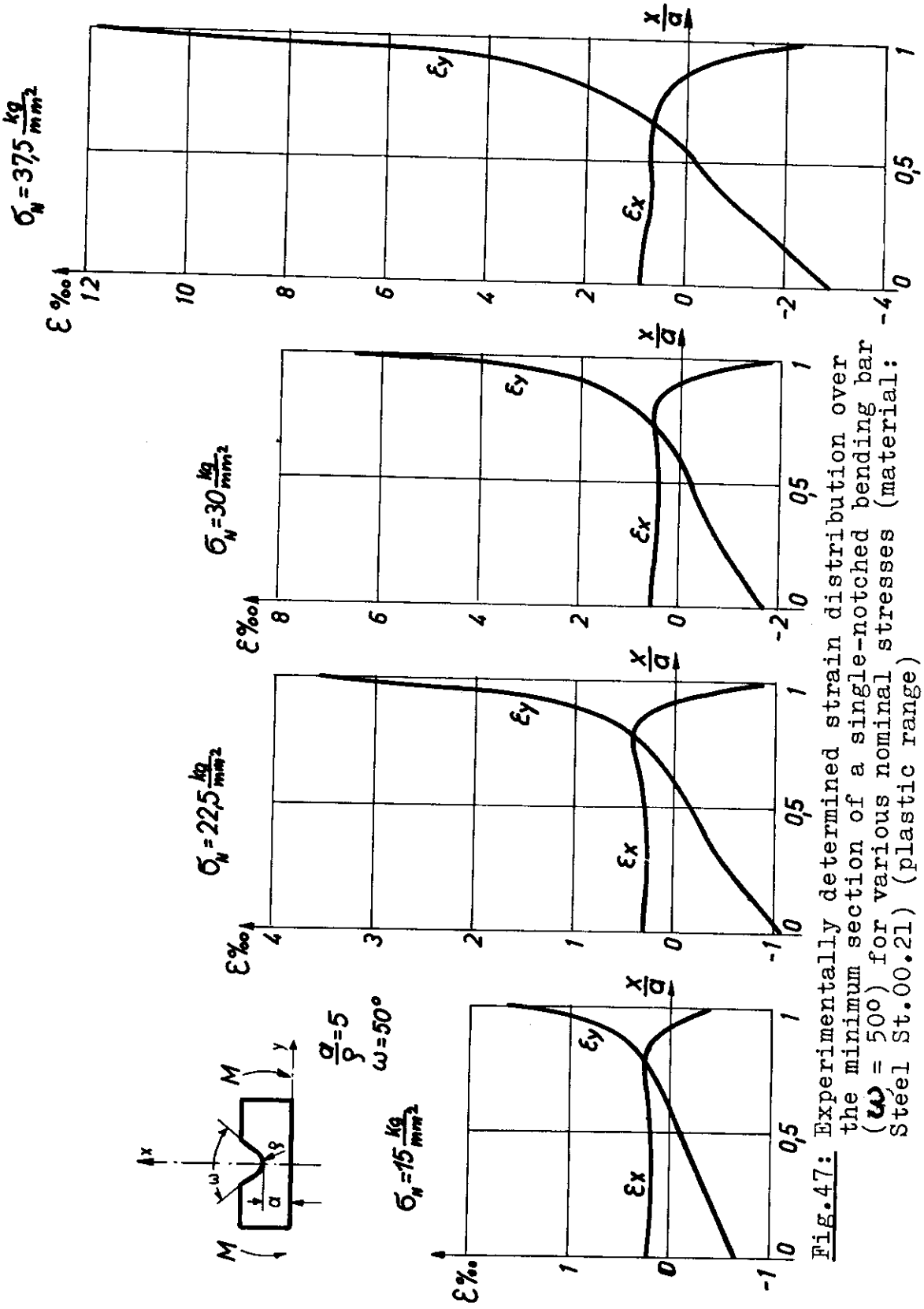

Fig.47: Experimentally determined strain distribution over the minimum section of a single-notched bending bar (ω = 50°) for various nominal stresses (material: Steel St.00.21) (plastic range)

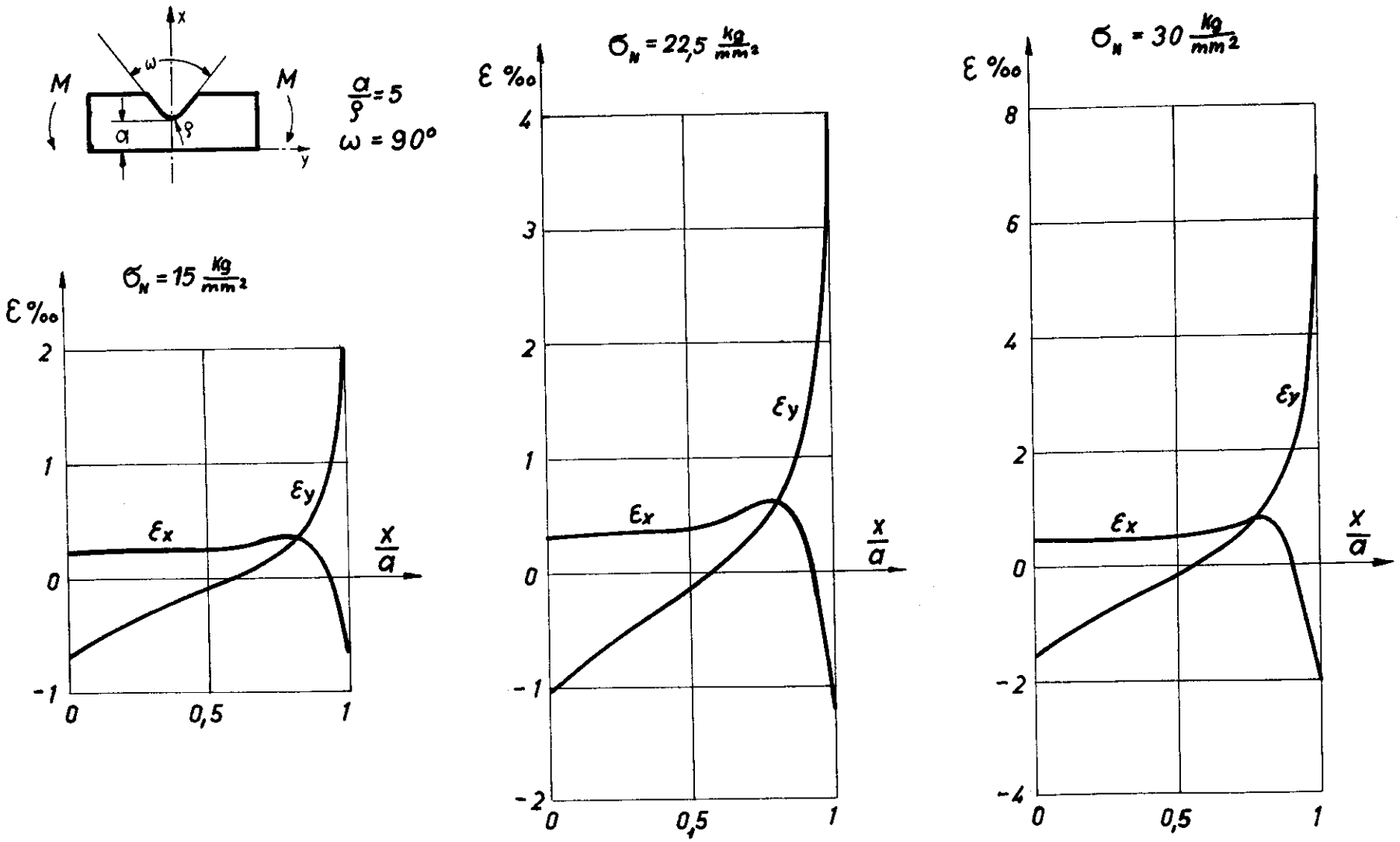

Fig.48: Experimentally determined strain distribution over the minimum section of a single-notched bending bar ($\omega = 90^{o}$) for various nominal stresses (material: Steel St.00.21) (plastic range)

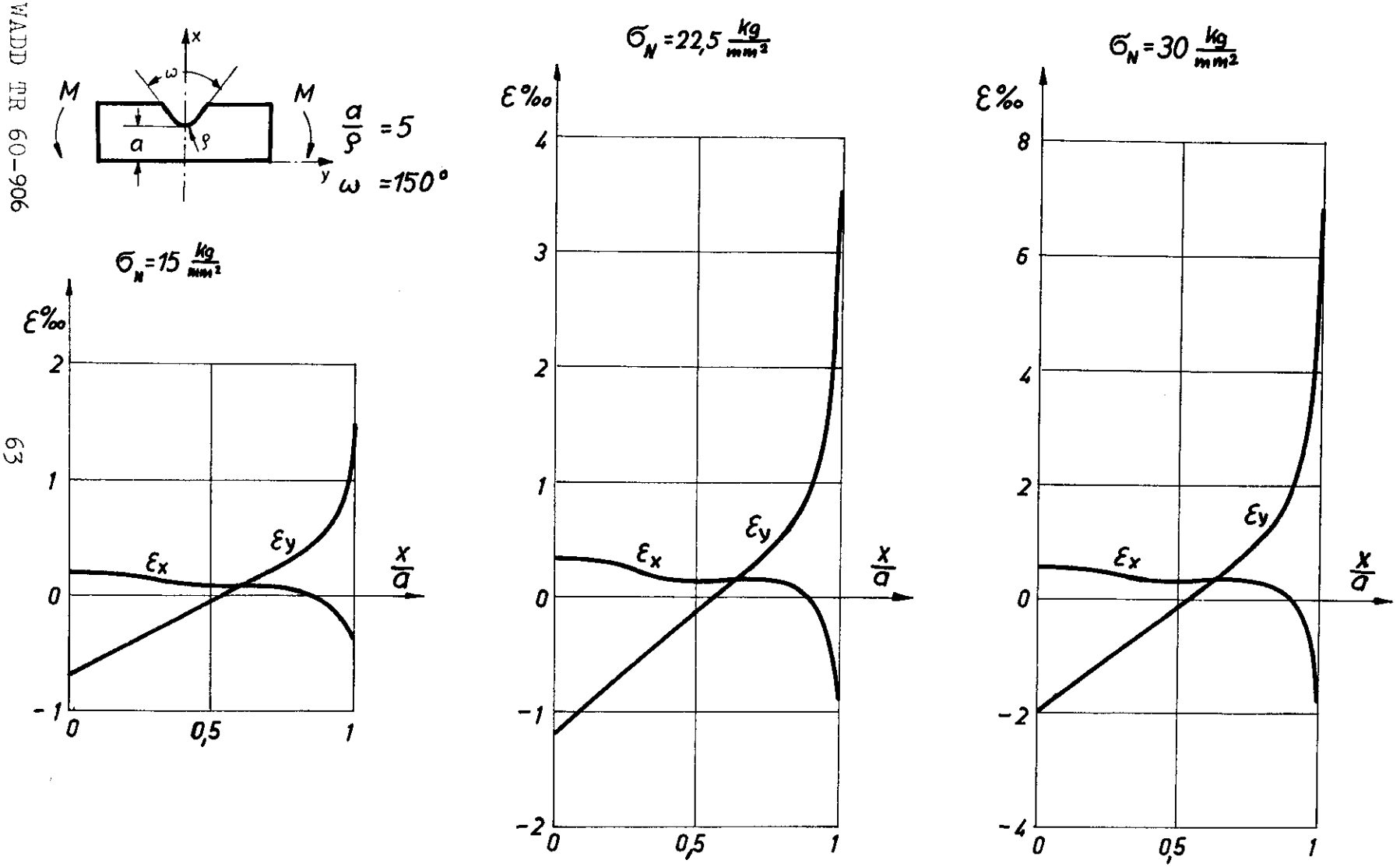

Fig.49: Experimentally determined strain distribution over the minimum section of a single-notched bending bar (ω = 150°) for various nominal stresses (material: Steel St.00.21) (plastic range)

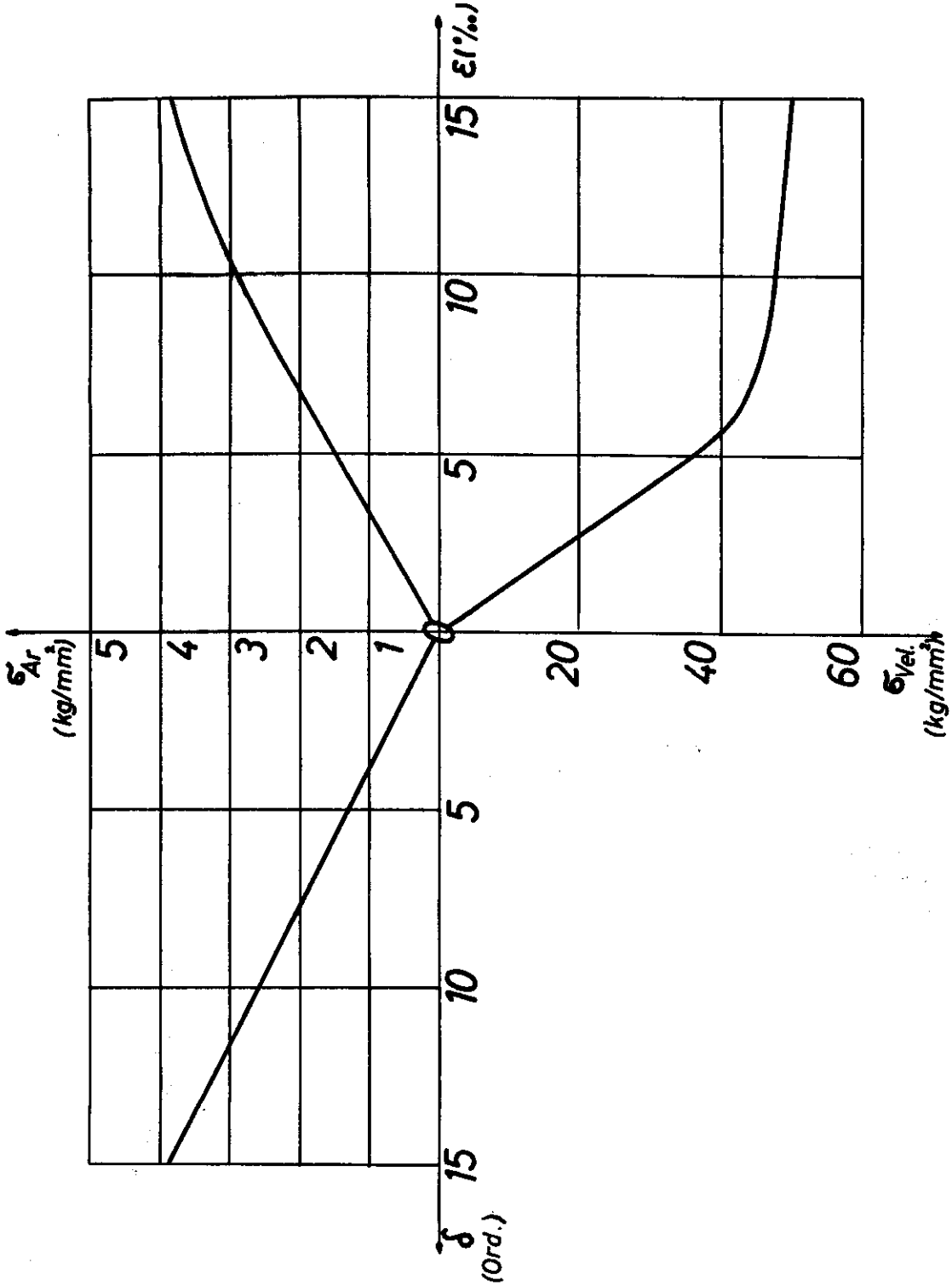

Fig.50: Nomogram for the analysis of the stress-coat experiments

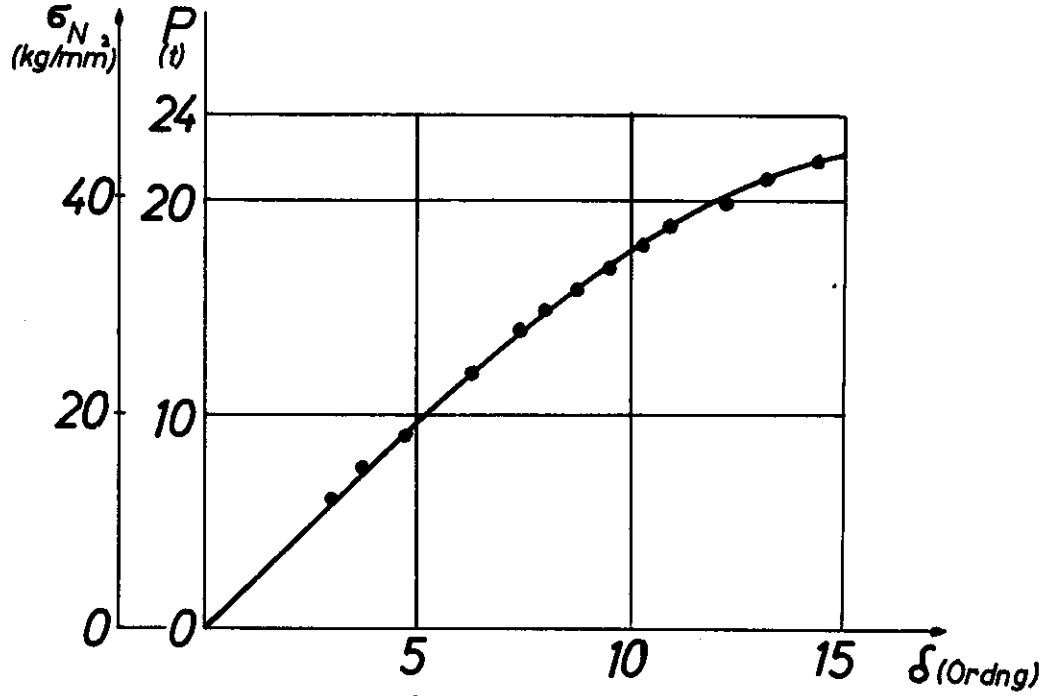

Fig.51: Fringe order δ vs. σ_N in the stress-coat test with Velodur

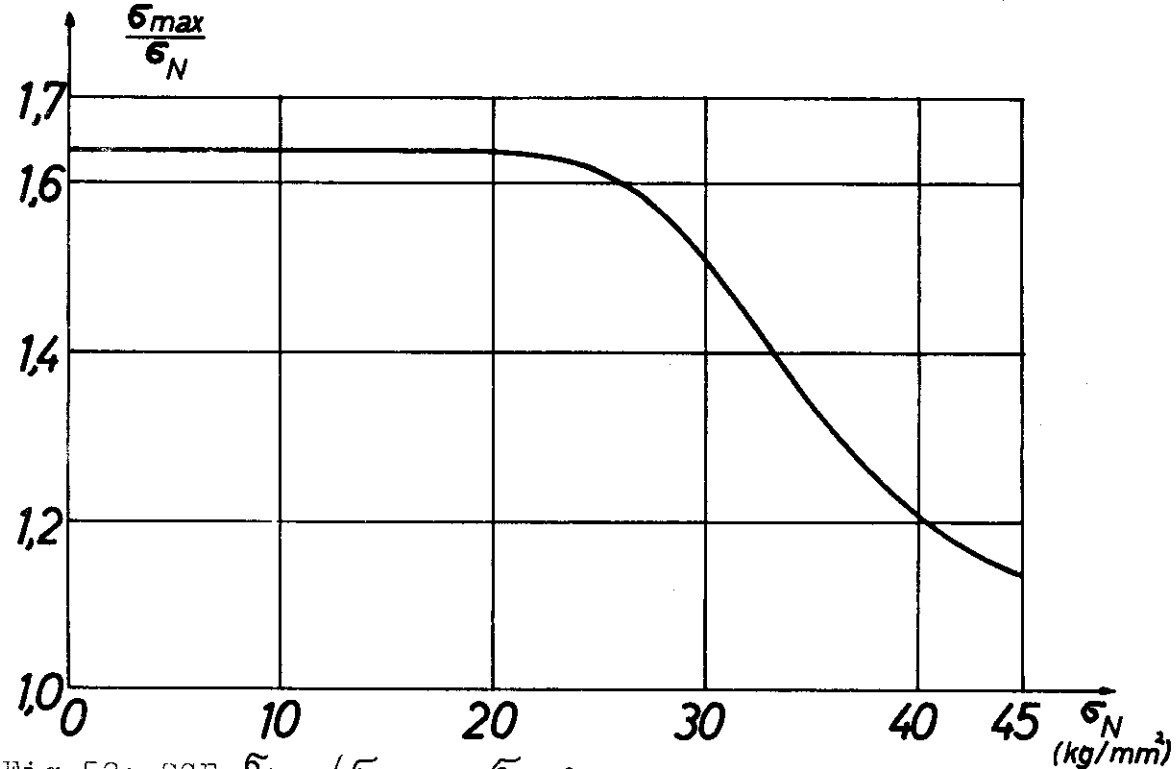

Fig.52: SCF σ_{MAX} / σ_N vs. σ_N for a tension strip with external notches (a/ρ = 1,0; material: Velodur), obtained by means of the stress-coat method

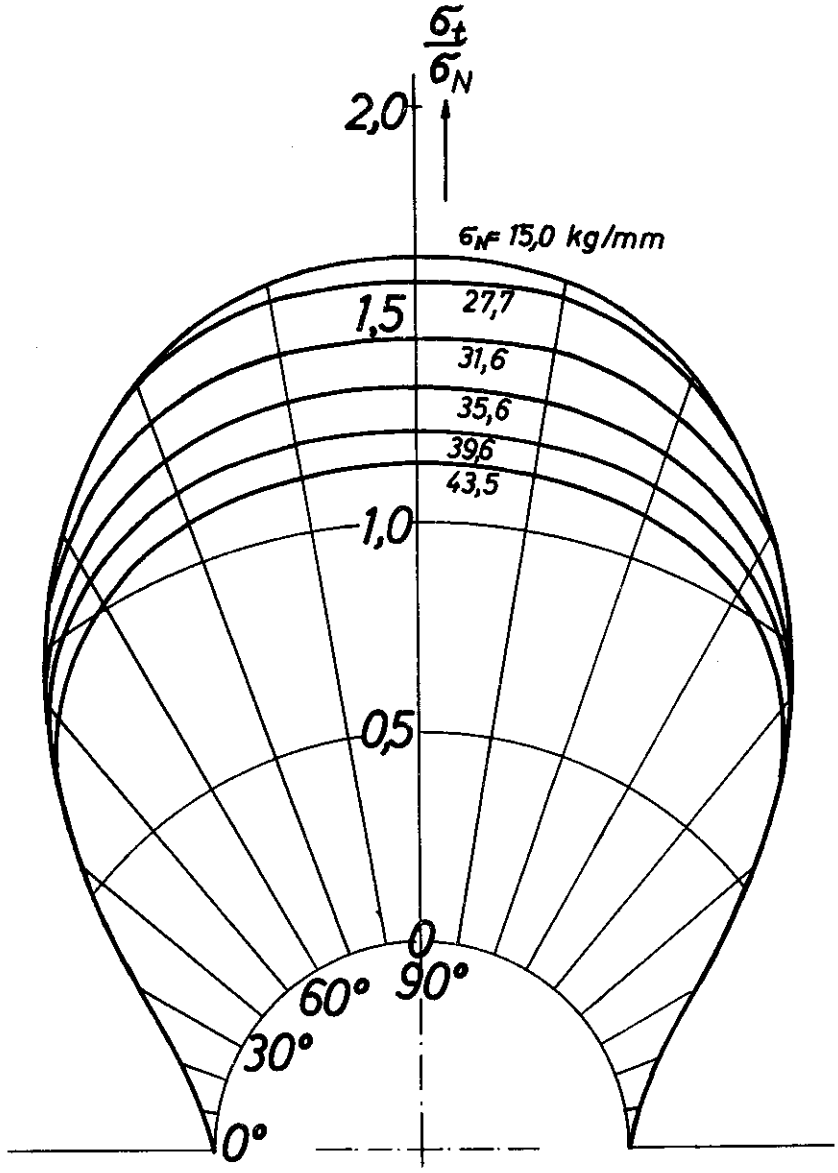

Fig.53: Stress distribution along the rim of the notch of a tension strip with external notches ($a/\rho = 1,0$; material: Velodur), obtained by means of the stress-coat method